NASA Contractor Report 2969

Analysis of Strong-Interaction Dynamic Stall for Laminar Flow on Airfoils

H. J. Gibeling, S. J. Shamroth,
and P. R. Eiseman

CONTRACT NAS1-13619
APRIL 1978

NASA

NASA Contractor Report 2969

Analysis of Strong-Interaction Dynamic Stall for Laminar Flow on Airfoils

H. J. Gibeling, S. J. Shamroth,
and P. R. Eiseman
United Technologies Research Center
East Hartford, Connecticut

Prepared for
Langley Research Center
under Contract NAS1-13619

National Aeronautics
and Space Administration

**Scientific and Technical
Information Office**

1978

TABLE OF CONTENTS

SUMMARY

In the present report a compressible Navier-Stokes solution procedure is applied to the flow about an isolated airfoil. Two major problem areas have been investigated. The first area is that of developing a coordinate system and an initial step in this direction has been taken. An airfoil coordinate system obtained from specification of discrete data points has been developed and the heat conduction equation has been solved in this system. Efforts required to allow the Navier-Stokes equations to be solved in this system are discussed. The second problem area is that of obtaining flow field solutions. Solutions for the flow about a circular cylinder and an isolated airfoil are presented. In the former case the prediction is shown to be in good agreement with data.

INTRODUCTION

The prediction of the flow field about isolated airfoils at various angles of attack has been a subject of great interest to aerodynamicists over the years. The importance of such flow fields is evident in the design of aerodynamic machinery. The associated aerodynamic problems vary from a whole machine to a detailed analysis of some constituent part. To name a few important problems, it is often necessary to determine from the flow field the performance of such components as an airplane wing, a control surface, a propeller or a helicopter rotor blade. In this context it should be clear that a reliable method of predicting aerodynamic flow fields is of great value.

In cases in which the airfoil is at a moderate angle of attack, the viscous boundary layer will remain attached over most of the airfoil surface; in these situations, lift and moment predictions as well as predictions of the detailed pressure distributions along the blade surfaces can be made with inviscid flow calculations such as those of Giesing (e.g., Ref. 1), Giesing, Kalman and Rodden (Ref. 2) or Bauer, Garabedian and Korn (Ref. 3). If skin friction drag for steady flows is desired, a boundary layer procedure such as those of Refs. 4 or 5 can be readily performed providing separation does not occur. For unsteady flows the incompressible procedures of Nash and Patel (Ref. 6) and Briley and McDonald (Ref. 7) are available. If separation does occur but the separation region remains small, predictions of the airfoil viscous layer can still be made, as has been demonstrated by Shamroth and Kreskovsky (Ref. 8) and Kreskovsky, Shamroth and Briley (Ref. 9) who applied the Briley-McDonald separation bubble calculation method to the problem of flow about an airfoil section with varying angle of attack.

The above procedures are applicable only in the absence of significant regions of separated flow. In many cases of practical interest the flow about the airfoil contains regions of significant separation, and in these cases procedures based upon an outer inviscid flow calculation which ignores viscous displacement effects and an inner viscous solution in the immediate vicinity of the airfoil are inapplicable.

An important example of an airfoil flow field which contains significant regions of separated flow is the helicopter rotor blade. It is this problem which has motivated the present study. Under high speed flight conditions the retreating rotor blades are subjected to a diminished dynamic pressure and as a result high blade performance requires large lift coefficients to be present over the retreating portion of the rotor disc. These large lift coefficients are generated by placing the blade at large incidence angles

relative to the oncoming velocity field. At these large incidences the boundary layers developing along the airfoil surface will separate over at least a portion of the chord. When separation becomes significant, the blade experiences a deterioration in performance and this deterioration is termed stall.

Airfoil stall can be divided into two main categories, static stall and dynamic stall. Static stall occurs when an airfoil is placed at a large incidence angle in a steady stream. This type of stall has been discussed in detail by McCullough and Gault (Ref. 10). Dynamic stall occurs when the incidence is a function of time. For example, as the helicopter rotor blade travels through the rotor disc, it may experience a varying incidence angle. Over most of the rotor disc the blade will be unstalled, however, stall may occur over a portion of the disc and over this portion the airfoil performance will suffer. Dynamic stall differs from static stall in two obvious ways. First of all, experimental evidence clearly shows that both the maximum lift obtainable and the incidence at which performance first deteriorates are greater under dynamic conditions than under static conditions (e.g., Ref. 11). Secondly, although under static conditions lift is uniquely related to incidence, the dynamic stall process has a hysteresis loop associated with it so that the lift depends upon the incidence history. This historical phenomena makes the dynamic stall process much more difficult to predict than static stall process.

Despite its complex nature dynamic stall has been the subject of several recent experimental investigations. For example, the behavior of the leading edge separation bubble has been investigated by Velkoff, Blaser and Jones (Ref. 12) and Isogai (Ref. 13) and the mechanism of dynamic stall on a NACA 0012 airfoil has been investigated by McCroskey and Philippe (Ref. 14), McCroskey, Carr, and McAlister (Ref. 15) and Parker (Ref. 16). The variation of lift and moment coefficients through the stall regime has been presented in several works such as those of Liiva (Ref. 11) and Landgrebe and Bellinger (Ref. 17).

Although dynamic stall may occur in a variety of flow situations it plays a particularly important role in helicopter rotor performance, particularly since a rotor blade may encounter a continuously varying free stream velocity and a continuously varying incidence angle as it proceeds around the rotor. Obviously the blade performance in terms of lift and moment coefficients will depend upon how the blade reacts to its changing environment. In addition, blade fatigue stress, blade flutter and aircraft vibration will be dependent upon the periodic blade loading and unloading. Thus the aerodynamic performance, the rotor structural integrity and aircraft vibration characteristics are all significantly affected by possible dynamic stall phenomena.

To date a variety of approaches have been used to analyze and predict dynamic stall. Since the various approaches have been motivated by different immediate objectives, the obvious differences in philosophy which have appeared are not surprising. A recent review of many of these methods has been given by McCroskey in Ref. 18. Ham and Garelick (Ref. 19) and Ham (Ref. 20) have attempted to model dynamic stall by an inviscid process in which vortices are shed from the airfoil leading edge. Although the theory has predicted maximum lift and moment coefficients during dynamic stall, it has not predicted the dynamic stall loop. Furthermore, in this approach the time or incidence at which stall begins either must be assumed arbitrarily or must be based upon a data correlation. Baudu, Sagner and Souquet (Ref. 21) also have developed an approach based upon a vortex shedding model.

Other investigators have approached the problem by building semi-empirical models of the stall process. These models have been motivated by the need for practical prediction techniques and have proven quite useful in predicting dynamic stall characteristics. For example, Ericsson and Reding have developed a procedure which predicts dynamic stall characteristics by combining static airfoil data with semi-empirical models (Refs. 22 and 23). Another example of this type of work is that of Lang (Ref. 24) who developed a prediction procedure which combines a bubble bursting criteria with an inviscid flow analysis. Although these methods serve a pressing practical need, their empirical nature dictates that they be used with caution. Still another approach predicts dynamic stall characteristics from data correlations. For example, Carta, Commerford and Carlson have related stall characteristics to the time-incidence history of the airfoil (Ref. 25). However, since this method is based upon data correlation for specific airfoils in specific types of motion, it is not clear how this method could be extended either to alternate airfoil shapes or to other types of motion.

Although the previously mentioned procedures fill an important immediate need, they are limited by semi-empiricism or dependence upon data correlations. A basic understanding of the stall process or the ability to make predictions well outside the correlating data base requires more fundamental approaches and several such approaches have been developed. For example, the analysis of Scruggs, Nash and Singleton (Ref. 26) treats fully turbulent boundary layer flow developing under a prescribed pressure gradient obtained from the full inviscid equations. The analysis has as its main objective an assessment of the effect of unsteady phenomena upon the trailing edge separation point. A more comprehensive analysis has been developed by Crimi and Reeves (Ref. 27) who combined linearized potential flow equations with boundary layer equations to predict the flow field behavior. While this procedure has had some success in predicting lift and moment hysteresis loops through stall, the model has several shortcomings. First, although the Crimi-Reeves approach uses a finite-difference boundary layer calculation in

regions of attached flow, it resorts to an integral procedure in the reversed flow region. In addition, the procedure uses a linearized inviscid analysis and empirical transition and bubble bursting criteria. In a recent work Shamroth and Kreskovsky (Ref. 8) have developed a weak interaction dynamic stall analysis which is not limited by integral boundary layer assumptions, semi-empirical bubble bursting assumptions and semi-empirical transition assumptions. In this work Shamroth and Kreskovsky applied the Briley-McDonald separated flow finite-difference code (Ref. 7) in conjunction with the Giesing potential flow code (Ref. 1) to analyze the dynamic stall problem. Although the procedure's weak interaction limitation prevented the code from calculating hysteresis loops through stall, the analysis did predict what appears to be the correct stall mechanism for a NACA 0012 airfoil oscillating at a Reynolds number of approximately 0.5×10^7. At the time of the Shamroth-Kreskovsky study it was commonly assumed such an airfoil would stall as a result of leading edge bubble bursting, however, Ref. 8 predicted the bubble to remain attached and stall to originate through abrupt separation of the turbulent boundary layer. This stall mechanism has been confirmed by the experiments of McCroskey, Carr and McAlister (Ref. 15) and Parker (Ref. 16), and as pointed out in Ref. 15 such behavior is consistent with the static data of Gregory and O'Reilly (Ref. 28) and Ridder (Ref. 29).

Despite the fact that both the Crimi-Reeves analysis and the Shamroth-Kreskovsky analysis approach the problem from a fundamental basis, both analyses are still limited by their treatment of the interaction between the inner viscous layer and the nominally inviscid flow. The Shamroth-Kreskovsky analysis does not allow any interaction and thus cannot be applied in regions of significant viscous separation. Although the Crimi-Reeves analysis includes an interaction model, this model is based upon a semi-empirically determined pressure in regions of separated flow. In addition, it should be recalled that the Crimi-Reeves inviscid analysis is based upon linearized theory. These considerations indicate the need for new analyses not limited by interaction models and an obvious candidate analysis fulfilling this requirement would be the full Navier-Stokes equations.

With the continued improvements in computers and the continued rapid advancement in numerical techniques, Navier-Stokes procedures have become an increasingly attractive alternative for calculating the flow about an airfoil. Much early work in this area concentrated upon predicting flow about a circular cylinder and a comprehensive bibliography on this subject can be found in the recent paper by Coutanceau and Bouard (Ref. 30). It should be noted that those works mentioned in Ref. 30 include solutions of both the steady state and time-dependent equations, however, all the procedures were limited to incompressible flow. More recently, Navier-Stokes

procedures have been applied to more complex shapes including airfoils (Refs. 31-32, 34). In Ref. 31 Mehta and Lavan have investigated the flow field about an impulsively started airfoil with a finite difference procedure using stream function and vorticity as dependent variables. These results gave an excellent picture of the starting process. However, the Mehta-Lavan procedure is limited to incompressible flow and has been applied only in conjunction with a conformal mapping procedure. In addition, the large number of relaxation iterations required per time step may give relatively long running times. According to Ref. 32, the run times for this method averaged 9.5 minutes of UNIVAC 1108 time per time step. Despite this relatively long run time, the excellent results of Ref. 31 represent a strong argument for Navier-Stokes solutions.

In another analysis, Wu and Sampath (Ref. 32) have applied the Wu-Thompson integro-differential formulation (Ref. 33) to the airfoil problem. This calculation also has shed light on the impulsively started airfoil problem, however, it is not easily extendable to compressible flow and to date it has been formulated and used only for an airfoil which can be mapped conformally into a circle. In addition, the procedure requires continuously more run time as the rotational portion of the flow field grows. This makes the procedure less attractive for predicting steady state solutions than for predicting transients. A different approach has been taken by Verhoff (Ref. 34) who has applied MacCormack's fully explicit method (Ref. 35) to the airfoil problem. Unlike the procedures of Refs. 31 and 32, this formulation is compressible, however, being fully explicit the procedure requires many time steps to convergence leading to relatively long run times. It is likely that this run time problem could be alleviated if MacCormack's more recent technique were used (Ref. 36).

Finally, in a recent paper Steger (Ref. 37) has used a viscous analysis in conjunction with the coordinate generation procedure of Thompson, Thames and Mastin (Ref. 38) to predict flow about an airfoil. The viscous analysis is that of Beam and Warming (Ref. 39) which follows Briley and McDonald (Ref. 40) in combining a Taylor expansion linearization with a Douglas-Gunn ADI procedure. The major difference in the two approaches lies in the choice of dependent variables. The same linearization was used with an alternate ADI approach by Lindemuth and Killeen (Ref. 41). The basic coordinate generation procedure (Ref. 38) depends upon the solution of an elliptic set of partial differential equations. Additional modifications are made in one coordinate direction so that mesh points are concentrated near the body surface and in the wake region near a specified branch cut. The branch cut, however, cannot be technically treated as a branch cut in the usual sense. The problem here occurs because only

function boundary conditions have been applied along the cut; the result is a cut with tangent discontinuities in the crossing coordinate curves. The simultaneous application of both function and derivative conditions would certainly remove this problem. However, it would also require the solution of a higher order elliptic system: a process which would be costly and inefficient. By contrast, the methods developed in this study can efficiently and correctly model the branch cut with both function and derivative specifications.

The work under the present effort represents the first step in obtaining a general efficient computer code capable of predicting flow about airfoils of general geometry. The work is an extension of the original work of Briley and McDonald (Ref. 41) for the numerical method and of Eiseman (Ref. 42) for the geometry. Although at present only two-dimensional, laminar flows are considered, the procedure is extendable both to three dimensions and to turbulent flows.

LIST OF SYMBOLS

Except where dimensions are specified, all quantities in the following are nondimensional; physical velocities are normalized by u_r, density by ρ_r, pressure by $\rho_r u_r^2$, dynamic viscosity by μ_r, and time by (L/u_r) where L is the reference length.

a	Speed of sound; m/sec
A	Constant defined in Eq. (13); Coordinate system parameter, Eq. (15); Matrix coefficient, Eq. (25b)
b	Major to minor axis ratio of ellipse
B	Constant defined in Eq. (13); Coordinate distribution parameter
c	Speed of light; m/sec
ds	Differential element of arc length
dy^i	Differential increment of coordinate y^i
D	Diameter of circular cylinder
D_m, D_m^2	Finite difference operators for coordinate y^m
$D_{\alpha\gamma}^{\beta\epsilon}$	Momentum equation coefficient, Eq. (13)
$\mathcal{D}$	Multidimensional spatial derivative operator vector
$\mathcal{D}_m$	Spatial derivative operator vector associated with coordinate y^m
$\vec{e}_i$	Coordinate tangent vector field, $\partial\vec{x}/\partial y^i$
$E_{\alpha\gamma}^{\beta}$	Momentum equation coefficient, Eq. (12)
F	General function, Eq. (20)
$F_{ij\alpha}^{\beta}$	Momentum equation coefficient, Eq. (13)

g_{ij}	Metric tensor coefficient
g^{ij}	Inverse metric tensor coefficient
G	General function, Eq. (20)
$G_{\alpha ij}$	Momentum equation coefficient, Eq. (13)
h_i	Metric coefficient, orthogonal coordinates
H	General vector function, Eq. (19)
$I_{\alpha\nu}$	Momentum equation coefficient, Eq. (13)
J	Jacobian
K	Momentum equation coefficient, Eq. (13)
ℓ	Number of nonlinear equations solved; Airfoil chord length
L	Reference length, meters
$L^{\omega}_{\alpha\nu}$	Momentum equation coefficient, Eq. (13)
$\mathcal{L}$	Linear operator, Eq. (25c)
m	Coordinate distribution parameter, Eq. (16)
M	Major axis of ellipse
M_r	Reference Mach number
$M_{\alpha\beta}$	Momentum equation coefficient, Eq. (13)
$\hat{n}$	Unit normal vector
p	Static pressure

Q^{β}_{γ}	Momentum equation coefficient, Eq. (11)
r	Coordinate parameter, Eq. (16)
R	Coordinate distribution function, Eq. (16)
R_{α}	Momentum equation coefficient, Eq. (13)
Re	Reference Reynolds number, $\rho_r u_r L/\mu_r$
s_i	Arc length along coordinate y^i
$s_{1_{max}}$	Total surface arc length
S	General vector function, Eq. (19)
S_{α}	Momentum equation coefficient, Eq. (13)
t	Time; Coordinate parameter, Eq. (15)
T_o	Total temperature
T^k_i	Stress-energy tensor, Eq. (5)
u	Streamwise cartesian velocity component
u_i	Physical velocity component along coordinate y^i
$\hat{u}_1, \hat{u}_2$	Cartesian unit vectors
v	Transverse cartesian velocity component
$\vec{v}$	Space-time velocity
v_i	Covariant velocity component
v^k	Contravariant velocity component

LIST OF SYMBOLS (CONT'D)

$\vec{x}, x^i$	Cartesian position vector
x_m	Arbitrary computational coordinate
$\vec{y}, y^m$	Computational coordinates
$\vec{\alpha}$	Outer loop position vector, Eq. (15)
α	Spatial differencing parameter, Eq. (29)
$\vec{\beta}$	Inner loop position vector, Eq. (14)
β	Time differencing parameter
γ	Ratio of specific heats, C_p/C_v
δ_i^j	Kronecker delta
Δt	Time increment
Δx_m	Mesh spacing for coordinate x_m
Δy^m	Mesh spacing for coordinate y^m
Δ_+, Δ_-	Spatial difference operators, Eq. (29)
θ	Polar coordinate
μ	Dynamic viscosity
ν	Kinematic viscosity; m^2/sec
ρ	Density
ϕ	General dependent variable
ψ	General dependent variable, Eq. (24)
ω_m	Fourth-derivative dissipation coefficient, Eq. (34)

Subscripts

∞	Denotes free stream conditions
r	Denotes dimensional reference value

Superscript

n	Denotes time level n

ANALYSIS

The Governing Equations in General Tensor Form

The role of generalized coordinates. - In the numerical solution of fluid dynamic problems there are many advantages to be gained by judicious choice of coordinates (eg., Ref. 43). The most obvious advantage is that the physical boundaries of a flow region can be represented by coordinate surfaces. This removes the need for fractional cells in general; hence, the complications and loss of accuracy associated with a boundary interpolation are removed. Another advantage is that a uniform numerical method can be used. The solution can then be performed with a fixed number of cells in any given direction and with a uniform mesh spacing. The result is a simplification of the computer logic; hence, a savings in time for both the computer and the programmer results.

In addition, the coordinate transformation can be constructed to contain distributions for physical space mesh points. In this context, the uniform mesh of computational space is simply mapped into a suitably distributed mesh in physical space. The resolution of large solution gradients is the major objective in the selection of a coordinate mesh distribution. A classical example is the resolution of attached boundary layers. Another more subtle example is the resolution of large gradients in computational coordinates due to regions of high curvature on the bounding surfaces. When the transformation contains the mesh point distribution there is no need to construct the apparatus for the discrete approximation of derivatives on a nonuniform mesh. This results in a savings in both computer logic and storage. As an illustration, consider the case where it is desired to automate the difference molecule so that the numerical technique can be changed with a few parameters. Changes, in practice, usually amount to a selection between forward, backward, or central differences. For any given direction, three parameters each for first and second derivatives are needed for second order accurate methods. Thus, counting 6 parameters for boundary conditions, a total of 12 parameters are needed for each ADI direction. This compares favorably with the direct approximation of derivatives on a nonuniform mesh where the requirement is for 6N parameters on an ADI direction of length N.

A further advantage of the generalized coordinate approach is that for a given problem coordinates can be selected from a large class of coordinate systems. In the process of sorting through the various possible coordinate systems two criteria arise. First, the new coordinates must lead to a real simplification; secondly, the coordinates must be easily generated.

Since bounding surfaces usually become coordinate surfaces the first criterion is almost always met. The remaining complexity in the first criterion is directly measured by consideration of the metric tensor (g_{ij}) which is obtained from the expression for the fundamental element of arc length

$$(ds)^2 = g_{ij}\, dy^i\, dy^j \tag{1}$$

Specifically, an increase in the number of nontrivial elements in the expression of the metric tensor is accompanied by a corresponding increase in the number of terms in the equations of motion. The result is an increase in the computational work that is needed after the coordinates have been generated along with the necessary metric data. The second criterion, unlike the first, is most often neglected. The unfortunate result is that there is often more work involved in making the coordinates than in solving the original problem with a less efficient satisfaction of the first criterion. In fact, both of the criteria above usually are at opposite polarities in complexity. The prudent selection of coordinates is then a balance between these criteria.

The criteria for selecting a suitable system of coordinates can be used to compare the various classes of coordinate systems and to evaluate the relative utility of each. The evaluation will start with conformal transformations and continually enlarge the class until the most general time-dependent coordinates are reached.

For conformal transformations the metric tensor is simply given by a scalar multiple of the identity. That is, $g_{ij} = h(\vec{y})\delta_{ij}$ where the Kronecker symbol δ_{ij} vanishes unless $i = j$ in which case it is unity. From this expression it is easy to show that $h = (J^2)^{1/n}$ where J is the Jacobian of the n-dimensional conformal transformation. The simplicity of the metric leads to very simple equations of motion at the expense of greatly restricting the class of easily obtained transformations. These transformations are generally obtained by the solution of partial differential equations which may in itself be costly. In addition, the control over the mesh distributions is indirect at best. In two dimensions, however, conformal transformations have been successfully used on many occasions. Here the metric is given by $g_{ij} = |J|\, \delta_{ij}$, and the theory of functions of one complex variable is a powerful tool which can be used. When the boundaries of the flow region can be matched with well-known conformal transformations there is nothing that can effectively compete with this way of generating coordinates.

In a number of cases boundaries can be matched through a sequence of well-known transformations. However, in most cases of practical importance

the boundaries are too complicated; and consequently, cannot be simply defined as desired. Thus, one is led to approximate methods. For the general airfoil shapes there is the method of Theodorsen (Ref. 44) and along similar lines there is the more recent work of Ives (Refs. 45, 46) which employs the Fast Fourier Transform. Both techniques map airfoils to near circles through a sequence of well-known maps; and then use a Fourier type of approximation. The Schwartz-Christoffel transformation may be used to approximate arbitrary shapes with piecewise linear curves. This technique works best for simply connected regions where no branch cuts are needed. A basic limitation in this method is the poor representation of wall curvature. This can be partially resolved by using the Schwartz-Christoffel transformation with rounded corners as in Henrici (Ref. 47). But then there is little control over the rounding process. Conformal mappings in higher dimensions also exist (cf., Ref. 48) but are generally difficult to construct.

When conformal mappings become overly difficult to construct, it is best to consider the slightly larger class of orthogonal transformations. For orthogonal transformations the metric tensor is given by the diagonal form $g_{ij} = \left[h_i(\vec{y})\right]^2 \delta_{ij}$. Note that, unlike the conformal transformations, the diagonal entries of the metric can be different. The deviation from conformality can now easily be measured by an examination of the ratios of the functions h_i as now is demonstrated by an explicit geometric interpretation of the metric. For a position vector field $\vec{x}$, the vector field $\vec{e}_i = (\partial\vec{x})/(\partial y^i)$ is the natural tangent vector field along coordinate curves generated by holding the remaining coordinates $y^1, \ldots, y^{i-1}, y^{i+1}, \ldots, y^n$ constant. It is often common practice to use the operator notation where the position vector field is omitted. By an application of the chain rule, the fundamental element of arc length can be expanded as

$$(ds)^2 = d\vec{x} \cdot d\vec{x} = \left(\frac{\partial \vec{x}}{\partial y^i}\, dy^i\right) \cdot \left(\frac{\partial \vec{x}}{\partial y^j}\, dy^j\right)$$
$$= \frac{\partial \vec{x}}{\partial y^i} \cdot \frac{\partial \vec{x}}{\partial y^j}\, dy^i dy^j = (\vec{e}_i \cdot \vec{e}_j)\, dy^i dy^j \qquad (2)$$

and hence, by linear independence $g_{ij} = \vec{e}_i \cdot \vec{e}_j$. Now note that the metric is orthogonal if and only if the $\vec{e}_i$ and $\vec{e}_j$ are perpendicular when $i \neq j$. But perpendicularity of $\vec{e}_i$ and $\vec{e}_j$ at a point is equivalent to the perpendicular crossing of the associated coordinate curves at the point in question. Consequently the notion of orthogonality in terms of coordinate curves is equivalent to the metric expression above. In addition the functions h_i are easily seen to be equal to the lengths of the corresponding natural tangent vectors $\vec{e}_i$. When the lengths are equal it is clear that the transformation is conformal. However, as the ratios of the h_i deviate from unity, the transformation smoothly deviates from conformality.

With fewer constraints on the metric, the selection of coordinates from the class of orthogonal transformations is slightly less restrictive than a selection from the class of conformal transformations. The process of coordinate generation is usually accomplished by geometric methods. The desire is to create families of mutually orthogonal coordinate surfaces. As a starting point, one usually begins the process with a given family of surfaces that are generated in some way from the boundary of the flow region. Families of orthogonal surfaces are then to be constructed to complete the specification of coordinates. The first family of surfaces defines a unique normal vector field. This vector field is then extended to a smooth field of orthogonal frames which must be integrated to generate the orthogonal coordinate surfaces. The condition for integrability is contained in the Frobenius Theorem (Ref. 49). The computational process generally leads to the solution of a system of differential equations. This, however, is often a difficult exercise just to obtain orthogonal coordinates.

General nonorthogonal coordinates are often preferable to orthogonal coordinates since the mesh distributions can be controlled and since the coordinates are considerably easier to generate. The construction process is usually geometric and generally does not rely on the solution of differential equations. Certain methods, however, are not entirely based upon the geometry, but upon the solution of a system of elliptic partial differential equations (e.g., Ref. 38). Such methods are generally of comparable efficiency with those of the conformal type. The entirely geometric methods usually can be used with distribution functions replacing independent variables so that mesh point distributions are used directly. Such is generally not the case for other methods. The considerable improvement in flexibility associated with the class of general spatial coordinates does come with a small price. Specifically, the metric tensor has generally nontrivial off diagonal elements. As with the difference between orthogonal and conformal coordinates, the deviation of the general nonorthogonal coordinates from orthogonality can be measured directly from the metric. That is, the cosine of the angle between distinct coordinate curves

is given by the dot product of the associated unit tangent vectors. The cosine of the angle between curves i and j can be written as:

$$\left(\frac{\vec{e}_i}{|\vec{e}_i|}\right)\cdot\left(\frac{\vec{e}_j}{|\vec{e}_j|}\right) = \frac{\vec{e}_i \cdot \vec{e}_j}{\sqrt{(\vec{e}_i \cdot \vec{e}_i)(\vec{e}_j \cdot \vec{e}_j)}} = \frac{g_{ij}}{\sqrt{g_{ii}\, g_{jj}}} \tag{3}$$

Thus when g_{ij} vanishes for distinct i and j the coordinates are orthogonal, and when g_{ij} increases from 0 the coordinates smoothly deviate from orthogonality with the deviation given by the arc cosine of Eq. (3). Local regions of nearly orthogonal coordinates can then be constructed within a nonorthogonal system. This can be used to some advantage in regions where large solution gradients are expected. For example, boundary layer regions may be treated with nearly orthogonal coordinates which smoothly deviate from orthogonality as largely inviscid regions are approached. An illustration of this type of construction is given in Ref. 42.

When time-dependent problems are considered the general nonorthogonal spatial coordinates can be used provided that the boundaries of the flow region are rigidly fixed relative to the region. However, if the region changes shape as a function of time, then the purely spatial coordinate analysis above is no longer valid unless special precautions are taken. In terms of the metric the pseudoriemannian metric from special relativity is used. Here, the cartesian frame x^1, x^2, x^3 is extended to a Lorentz frame by the addition of a time-like coordinate x^0 (Refs. 50-54). The fundamental expression for arc length in space-time is

$$(ds)^2 = g_{ij}\, dy^i\, dy^j \tag{4}$$

where the summation is now from 0 to 3.

In this context, the classical equations of motion are obtained from the vanishing divergence of the stress-energy tensor and a subsequent approximation for slowly moving fluids. This is discussed at more length in the following section. Possible applications for such coordinate systems include ducts with moving walls such as blood flow problems as well as flutter problems where airfoils may be oscillating relative to each other. As special cases the classical Eulerian and Lagrangian coordinates as well as everything in between are obtained.

The equations of motion for a viscous fluid. - The equations of motion of a viscous fluid are given by a divergence free stress-energy tensor

$$T_i^k = \rho v_i v^k + (p + \frac{2}{3}\mu \ \mathrm{div}\,\vec{v})\,\delta_i^k - \mu\, g^{mk}(v_{i,m} + v_{m,i}) \qquad (5)$$

(Refs. 50-54) where $\vec{v}$ is a space-time velocity, v_i are covariant components, v^k are contravariant components, μ is viscosity, p is pressure, ρ is density, commas denote covariant derivatives, g^{mk} is the inverse metric, and δ_i^k is the Kronecker delta. In tensor analysis, the term contravariant refers to the components of a vector in the basis $\vec{e}_i$; covariant, to the components of the vector in the basis $\vec{e}^j$ defined by the duality condition $\vec{e}_i \cdot \vec{e}^j = \delta_i^j$. Here the Latin indices generally vary from 0 to 3 and repeated indices are to be summed (Einstein summation convection). The metric is generated from a local Lorentz frame and generally depends upon the velocity of light c. Since the velocities in classical mechanics are much less than the velocity of light, the Navier-Stokes equations can be retrieved as an approximation to the equations

$$T_i^k{}_{,k} = 0 \qquad (6)$$

when terms of order c^{-2} relative to unity are removed. The advantage inherent in the approximation of the above special relativistic equation is that the Navier-Stokes equations are expressed in a manner independent of any space-time coordinate system and are given a metric structure induced from the relativistic structure. The metric structure contains the classical Coriolis and centrifugal force effects in a clean and concise manner. That is, in addition to spatial changes, the metric contains all of the time-dependent variations of the coordinate transformations. The details of the approximation were presented in McVittie (Ref. 50) for inviscid flows and in Walkden (Ref. 52) for viscous flows. All quantities in the following equations are nondimensional; physical velocities are normalized by u_r, density by ρ_r, pressure by $\rho_r u_r^2$, dynamic viscosity by μ_r, and time by (L/u_r) where L is the reference length. The resulting equations for viscous flow (Ref. 52) are

$$\frac{\partial}{\partial t}(\rho J) + \frac{\partial}{\partial y^\beta}(\rho v^\beta J) = 0 \qquad (7)$$

for i = 0 and

$$\frac{1}{J}\left[\frac{\partial}{\partial t}(\rho v_\alpha J) + \frac{\partial}{\partial y^\beta}\left\{\left[\rho v_\alpha v^\beta + (p + \frac{2}{3}\frac{\mu}{Re}\,\mathrm{div}\,\vec{v})\,\delta_\alpha^\beta\right.\right.\right.$$

$$\left.\left.\left. - \frac{\mu}{Re} g^{\epsilon\beta}\,(v_{\alpha,\epsilon} + v_{\epsilon,\alpha})\right] J\right\}\right] - \frac{1}{2}\,\frac{\partial g_{\epsilon\beta}}{\partial y^\alpha}\left[\rho v^\epsilon v^\beta + (p + \frac{2}{3}\frac{\mu}{Re}\,\mathrm{div}\,\vec{v})\,g^{\epsilon\beta}\right. \quad (8)$$

$$\left. - \frac{\mu}{Re} g^{\omega\epsilon}\, g^{\gamma\beta}\,(v_{\gamma,\omega} + v_{\omega,\gamma})\right] - \frac{1}{2}\,\rho\,\frac{\partial g_{oo}}{\partial y^\alpha} - \rho v^\beta \frac{\partial g_{o\beta}}{\partial y^\alpha} = 0$$

for i = 1, 2, 3 where J is the Jacobian. The equation for i = 0 can be identified as the continuity equation; the equations for $1 \leq i \leq 3$, as the respective momentum equations. Here, i = 0 represents the time-like direction and Greek indices α, β, ε, ω represent space-like directions as they vary only from 1 to 3. The energy equation, also presented in Ref. 52, can often be replaced with

$$p = \rho\left[A + B\, g_{ij}\, v^i v^j\right] \quad (9)$$

under an assumption of constant total temperature, where $A = T_o/\gamma M_r^2$ and $B = -(\gamma-1)/2\gamma$. An expansion of the momentum equation leads to a system of the form

$$\frac{\partial}{\partial t}(J\, g_{\alpha i}\, \rho v^i) + K\,\frac{\partial \rho}{\partial y^\alpha} + F_{ij\alpha}^{\beta}\,\frac{\partial}{\partial y^\beta}\,(\rho v^i v^j) + L^{\omega}_{\alpha\nu}\,\frac{\partial v^\nu}{\partial y^\omega}$$

$$+ D_{\alpha\gamma}^{\epsilon}\,\frac{\partial^2 v^\gamma}{\partial y^\beta\,\partial y^\epsilon} + R_\alpha\,\rho + I_{\alpha\nu} v^\nu + M_{\alpha\beta}\,\rho v^\beta + G_{\alpha ij}\,\rho v^i v^j = S_\alpha \quad (10)$$

which is suitable for automatic computation. For a time-independent metric, this result reduces to the Navier-Stokes equations in a fixed frame (Ref. 55). By use of the intermediate quantities

$$Q_\gamma^\beta = \delta_\gamma^\beta - g_{\gamma o}\, g^{o\beta} \quad (11)$$

and

$$E^{\beta}_{\alpha\gamma} = \frac{\mu}{Re}\left[\frac{2}{3}\,\frac{\partial J}{\partial y^{\gamma}}\,\delta^{\alpha}_{\beta} - J\,g^{\epsilon\beta}\,\frac{\partial g_{\alpha\epsilon}}{\partial y^{\alpha}}\right] \tag{12}$$

the coefficients of the above system are given by

$$K = AJ$$

$$F^{\beta}_{ij\alpha} = \left(g_{\alpha i}\,\delta^{\beta}_{j} + B g_{ij}\,\delta^{\beta}_{\alpha}\right) J$$

$$G_{\alpha ij} = \frac{\partial F^{\beta}_{ij\alpha}}{\partial y^{\beta}} - \frac{J}{2}\,\frac{\partial g_{\epsilon\beta}}{\partial y^{\alpha}}\left(\delta_{i}^{\ \epsilon}\,\delta^{\beta}_{j} + B g_{ij}\,g^{\epsilon\beta}\right)$$

$$M_{\alpha\beta} = -J\,\frac{\partial g_{o\beta}}{\partial y^{\alpha}}$$

$$R_{\alpha} = A\,\frac{\partial J}{\partial y^{\beta}}\,\delta^{\beta}_{\alpha} - \frac{J}{2}\left[\frac{\partial g_{oo}}{\partial y^{\alpha}} + A\,\frac{\partial g_{\epsilon\beta}}{\partial y^{\alpha}}\,g^{\epsilon\beta}\right]$$

$$D^{\beta\epsilon}_{\alpha\gamma} = \frac{\mu}{Re}\,J\left[\frac{2}{3}\,\delta^{\beta}_{\alpha}\,\delta^{\epsilon}_{\gamma} - g_{\alpha\gamma}\,g^{\epsilon\beta} - Q^{\beta}_{\gamma}\,\delta^{\epsilon}_{\alpha}\right]$$

$$S_{\alpha} = \frac{\mu}{Re}\,\frac{\partial g_{\epsilon\beta}}{\partial y^{\alpha}}\left[\frac{1}{3}\,g^{\epsilon\beta}\,\frac{\partial J}{\partial t} - \frac{J}{2}\,g^{\omega\epsilon}\,g^{\gamma\beta}\,\frac{\partial g_{\gamma\omega}}{\partial t}\right] \tag{13}$$

$$- \frac{2}{3}\,\frac{\partial}{\partial y^{\alpha}}\left(\frac{\mu}{Re}\,\frac{\partial J}{\partial t}\right) + \frac{\partial}{\partial y^{\beta}}\left(\frac{\mu}{Re}\,J\,g^{\epsilon\beta}\,\frac{\partial g_{\alpha\epsilon}}{\partial t}\right)$$

$$I_{\alpha\nu} = \frac{\partial E^{\beta}_{\alpha\nu}}{\partial y^{\beta}} + \frac{\frac{\mu}{Re}}{2}\,\frac{\partial g_{\epsilon\beta}}{\partial y^{\alpha}}\left[J\,g^{\omega\epsilon}\,g^{\gamma\beta}\,\frac{\partial g_{\gamma\omega}}{\partial y^{\nu}} - \frac{2}{3}\,\frac{\partial J}{\partial y^{\nu}}\,g^{\epsilon\beta}\right]$$

$$L^{\omega}_{\alpha\nu} = E^{\omega}_{\alpha\nu} + \frac{\partial D^{\beta\omega}_{\alpha\nu}}{\partial y^{\beta}} + \frac{\frac{\mu}{Re}\,J}{2}\,\frac{\partial g_{\epsilon\beta}}{\partial y^{\alpha}}\left[g^{\omega\epsilon}\,Q^{\beta}_{\nu} + g^{\omega\beta}\,Q_{\nu}^{\ \epsilon} - \frac{2}{3}\,g^{\epsilon\beta}\,\delta_{\nu}^{\ \omega}\right]$$

The Coordinate System

An effective coordinate system for the two-dimensional isolated airfoil problem can be generated from two loops (or arcs) of data. The two loops first are given a parameterization t in a manner which causes both a distribution of loopwise points and an alignment of points between the two loops. Here, the inner loop is the airfoil; the outer loop, the outer computational boundary. The coordinate system is then generated by a linear interpolation between loops. If $\vec{\alpha}(t)$ denotes an outer loop; $\vec{\beta}(t)$, an inner loop; and R(r), a distribution function with independent variable $0 \leq r \leq 1$; then the coordimate transformation is given by

$$\vec{x} = \vec{\beta} + R(\vec{\alpha} - \vec{\beta}) \tag{14}$$

where the cartesian location $\vec{x}$ is $\vec{\beta}$ when R = 0 and $\vec{\alpha}$ when R = 1. The metric data for this coordinate system is presented in Ref. 42 where the loops are constructed for a cascade of airfoils rather than for an isolated airfoil. Although the coordinate transformation, Eq. (14), is representative of a large class of transformations, it is instructive to specialize our discussion at least initially for purposes of illustration. Thus, in most of the discussion, it will be assumed that the airfoil has no cusps and is convex; minor modifications can be employed for cusps and regions of concavity. With convexity, an orthogonal coordinate system can be generated if each interpolation between inner and outer loop points is over a line normal to the airfoil surface. This can be accomplished by generating the outer computational boundary $\vec{\alpha}$ as a uniform dilation along airfoil normal lines. That is, if $\hat{n}(t)$ is the outward unit normal vector field to the airfoil $\vec{\beta}(t)$, then the outer computational boundary is given by

$$\vec{\alpha}(t) = \vec{\beta}(t) + A\hat{n}(t) \tag{15}$$

for some fixed distance A. The parameter t, as a loopwise distribution, can easily by specified as the arc length of some intermediate loop $\vec{\beta}(t) + B\hat{n}(t)$ where $0 \leq B \leq A$. The parameter t can be viewed as a label for corresponding inner and outer loop points. This is analogous to inner and outer points being displayed as sequences each with an index t. In taking the analogy one step further, the pseudoradial curves correspond to the lines joining inner and outer loop points with the same index. As B is adjusted from 0 to A the distribution varies from airfoil arc length towards outer loop arc length. Under a uniform discretization of t, this will cause points to cluster around the airfoil regions of higher curvature

(notably at leading and/or trailing edges) as A is approached. To complete the specificaiton of the coordinate transformation, Eq. (14), a definition of R(r) is needed. The function R(r) is used to specify a distribution of points along the coordinate curves normal to the airfoil. Commonly, it is desired to resolve a boundary layer near the airfoil surface. For this purpose, the distribution

$$R(r) = mr + (1-m)\left[1 - \frac{\tanh D(1-r)}{\tanh D}\right] \tag{16}$$

is most effective (Ref. 42). Here, a slope m is selected to determine a suitable uniform boundary layer mesh corresponding to the line R = mr; the level of adherence to this line is a result of the selected damping factor D. As D is increased from 0, the distribution will depart from global uniformity and more closely follow the given line before increasing to the end point R(1) = 1. By construction, the only inflection point occurs at R(1) = 1. Due to the inflection point condition, the distribution leaves an almost uniformly distributed boundary layer region with a continuously expanding grid as r approaches 1.

Once the coordinate transformation is established, the numerical solution for a desired flow field can be attempted. The mesh in the computational domain is given by uniform discretizations of both r and t. The array of mesh points here is a rectangular formation which is considerably simpler than the corresponding array in physical space. The advantages of this formulation are clear.

In certain cases the coordinate system can be constructed directly from an analytically specified airfoil surface. For example, consider an airfoil in the shape of an ellipse. The analytic specification is given by

$$\vec{\beta}(\theta) = \frac{M(\cos\theta\,\hat{u}_1 + \sin\theta\,\hat{u}_2)}{\sqrt{1+(b^2-1)\sin\theta}} \tag{17}$$

for $0 \le \theta \le 2\pi$ and where $\hat{u}_1$ and $\hat{u}_2$ are the standard cartesian unit vectors. The major axis is denoted by M; the ratio of major to minor axes, by b. If the outward expansion along the unit normals is sufficiently large (as is often the case), then the outer loop is nearly circular. As such, the distribution t determined by the outer loop arc length is, for all practical purposes, proportional to the angles formed by the outward unit normals and the x - axis. With a little algebra, it can be shown that

$$\theta = \tan^{-1}\left(\frac{\tan t}{b^2}\right) \tag{18}$$

which upon substitution leads to the desired parametric form of the airfoil $\vec{\beta}(t)$.

Generally, the coordinate construction must be done numerically. The process is broken down into a sequence of operations; namely, the determination of airfoil normals, the selection of B, the construction of inner and outer loops, and finally the generation of coordinates from R and the two loops. In more detail these operations are tabulated as follows:

(a) Generate the airfoil surface $\vec{\beta}(s)$ where s is an arc length parameterization.

(b) Construct the unit vector field $\hat{n}(s)$.

(c) Choose B such that $o \leq B \leq A$

(d) Construct the intermediate loop $\vec{\gamma}_B(s) = \beta(s) + B\,\hat{n}(s)$

(e) Store the paired points $(\vec{\beta}(s), \vec{\gamma}_B(s))$

(f) Reparameterize $\vec{\gamma}_B$ by its arc length t to obtain $\vec{\gamma}_B(t)$

(g) From the pairing in (e), reparameterize the airfoil surface to obtain $\vec{\beta}(t)$

(h) Generate the outer boundary from Eq. (15)

(i) Choose the number, N, of loopwise mesh points

(j) If t varies from o to some value T, then set $\Delta t = T/(N-1)$

(k) For each $t = n\Delta t$, evaluate inner and outer loops as $n = o,\ldots, N-1$

(l) Choose the parameters m and D which control the desired resolution for the boundary layer region

(m) Choose the number, M, of mesh points in the pseudoradial direction

(n) For each $r = m/(M-1)$, evaluate the radial distribution (Eq. (16)) for $m = o, 1,\ldots, M-1$

(o) Generate an NxM coordinate grid from Eq. (14), step (k) and step (n)

If the airfoil data is not smooth, then a least squares curve fit will be needed to determine the normals (Ref. 56). Further curve fits will be needed to construct inner and outer loops. If, however, B is not too large, then inner and outer loops can be constructed directly from a fit to the intermediate curve corresponding to B. Since the intermediate curve has an arc length parameterization it is usually easier to obtain an accurate fit. In any case, it is only necessary to fit one curve; the others can be obtained as expansions or contractions along the normal lines.

The method of coordinate construction presented here can also be adapted to the specific high Reynolds number problem considered by Steger (Ref. 37). In that problem the mesh was generated to resolve a flow field about an isolated airfoil with a long but narrow wake region. For this case, the leading edge region on the airfoil is considered to be bounded by the points above and below the airfoil where the outward unit normal vector first becomes vertical. The unit vector field $\hat{n}(t)$ is now chosen to coincide with the outward unit normal vector in the leading region, to point vertically outward in the remaining airfoil regions, and in continuation to point vertically away from a horizontal branch cut in the wake region. The result is two arcs of data rather than two loops of data. As before, the distribution t is determined by the arc length of an intermediate arc. The general construction and analysis of two loop (or arc) coordinate systems is given in Ref. 42. There the analysis includes coordinate stretches which are applicable to the wake region where an expanding mesh may be desired. An illustration of this coordinate system is given in Fig. 1.

The MINT Procedure

One of the major obstacles to the routine numerical solution of the multi-dimensional compressible Navier-Stokes equations is the large amount of computer time generally required, and consequently, efficient computational methods are highly desirable. Most methods for solving the compressible Navier-Stokes equations have been based on explicit difference schemes for the unsteady form of the governing equations and are subject to one or more stability restrictions on the size of the time step relative to the spatial mesh size. These stability limits usually correspond to the well known Courant-Friedrichs-Lewy (CFL) condition and, in some schemes, to an additional stability condition arising from viscous terms. In one dimension, the CFL condition is $\Delta t \leq \Delta x/(|u| + a)$, and the viscous stability condition is $\Delta t \leq (\Delta x)^2/2\nu$, where Δt is the time step, Δx is the mesh size,

u is the velocity, a is the speed of sound, and ν is kinematic viscosity. These stability restrictions can lower computational efficiency by imposing a smaller time step than would otherwise be desirable. Thus, a key disadvantage of conditionally stable methods is that the maximum time step is fixed by the spatial mesh size rather than the physical time dependence or the desired temporal accuracy. In contrast to most explicit methods, implicit methods tend to be stable for large time steps and hence offer the prospect of substantial increases in computational efficiency, provided of course that large time steps are acceptable for the physical problem of interest and that the computational effort per time step is competitive with that of explicit methods. In an effort to exploit these potentially favorable stability properties, an efficient implicit method based on alternating-direction differencing techniques was developed by Briley and McDonald (Ref. 40).

This method was subsequently designated the Multidimensional Implicit Nonlinear Time-dependent (MINT) solution procedure. The MINT method was further developed and applied to both laminar and turbulent duct flows by Briley, McDonald and Gibeling (Ref. 57). Subsequently, a three-dimensional compressible Navier-Stokes combustor flow analysis employing the MINT procedure was developed by Gibeling, McDonald and Briley (Ref. 58) and this procedure was then employed by Levy, et al., (Ref. 59) to determine the feasibility for computing a turbulent shock-wave boundary layer interaction with an implicit method.

Outline of method. - The MINT procedure has been previously described in Refs. 40 and 57, however, the description will be repeated here for completeness. The method can be briefly outlined as follows: the governing equations are replaced by an implicit time difference approximation, optionally a backward difference or Crank-Nicolson scheme. Terms involving nonlinearities at the implicit time level are linearized by Taylor expansion about the solution at the known time level, and spatial difference approximations are introduced. The result is a system of multidimensional coupled (but linear) difference equations for the dependent variables at the unknown or implicit time level. To solve these difference equations, the Douglas-Gunn (Ref. 60) procedure for generating alternating-direction implicit (ADI) schemes as perturbations of fundamental implicit difference schemes is introduced. This technique leads to systems of coupled linear difference equations having narrow block-banded matrix structures which can be solved efficiently by standard block-elimination methods.

The method centers around the use of a formal linearization technique adapted for the integration of initial-value problems. The linearization technique, which requires an implicit solution procedure, permits the

solution of coupled nonlinear equations in one space dimension (to the requisite degree of accuracy) by a one-step noniterative scheme. Since no iteration is required to compute the solution for a single time step, and since only moderate effort is required for solution of the implicit difference equations, the method is computationally efficient; this efficiency is retained for multidimensional problems by using ADI techniques. The method is also economical in terms of computer storage, in its present form requiring only two time-levels of storage for each dependent variable. Furthermore, the ADI technique reduces multidimensional problems to sequences of calculations which are one-dimensional in the sense that easily-solved narrow block-banded matrices associated with one-dimensional rows of grid points are produced. Consequently, only these one-dimensional problems require rapid-access storage at any given stage of the solution procedure, and the remaining flow variables can be saved on auxiliary storage devices if desired.

Although present attention is focused on the compressible Navier-Stokes equations, the numerical method employed is quite general and is formally derived for systems of governing equations which have the following form:

$$\partial H(\phi)/\partial t = \mathcal{D}(\phi) + S(\phi) \tag{19}$$

where ϕ is a column vector containing ℓ dependent variables, H and S are column vector functions of ϕ, and $\mathcal{D}$ is a column vector whose elements are spatial differential operators which may be multidimensional. The generality of Eq. (19) allows the method to be developed concisely and permits various extensions and modifications (e.g., noncartesian coordinate systems, turbulence models) to be made more or less routinely. It should be emphasized, however, that the Jacobian $\partial H/\partial\phi$ must usually be nonsingular if the ADI techniques as applied to Eq. (19) are to be valid. A necessary condition is that each dependent variable appear in one or more of the governing equations as a time derivative. An exception would occur if for instance, a variable having no time derivative also appeared in only one equation, so that this equation could be decoupled from the remaining equations and solved a posteriori by an alternate method. As a consequence, the present method is not directly applicable to the incompressible Navier-Stokes equations except in one dimension, where ADI techniques are unnecessary. For example, the velocity-pressure form of the incompressible equations has no time derivative of pressure, whereas the vorticity-stream-function form has no time derivative of stream function. For computing steady solutions, however, the addition of suitable "artificial" time derivatives to the incompressible equations, as was done in Chorin's (Ref. 61) artificial compressibility method, would permit the application of the present method.

Alternatively, a low Mach number solution of the present velocity-density formulation of the compressible equations can be computed.

Linearization technique. - A number of techniques have been used for implicit solution of the following first-order nonlinear scalar equation in one dependent variable $\phi(x,t)$:

$$\partial\phi/\partial t = F(\phi)\,\partial G(\phi)/\partial x \tag{20}$$

Special cases of Eq. (20) include the conservation form if $F(\phi) = 1$, and quasi-linear form if $G(\phi) = \phi$. Previous implicit methods for Eq. (20) which employ nonlinear difference equations and also methods based on two-step predictor-corrector schemes are discussed by Ames (Ref. 62, p. 82) and von Rosenburg (Ref. 63, p. 56). One such method is to difference nonlinear terms directly at the implicit time level to obtain nonlinear implicit difference equations; these are then solved iteratively by a procedure such as Newton's method. Although otherwise attractive, there may be difficulty with convergence in the iterative solution of the nonlinear difference equations, and some efficiency is sacrificed by the need for iteration. An implicit predictor-corrector technique has been devised by Douglas and Jones (Ref. 64) which is applicable to the quasilinear case ($G = \phi$) of Eq. (20). The first step of their procedure is to linearize the equation by evaluating the non-linear coefficient as $F(\phi^n)$ and to predict values of $\phi^{n+\frac{1}{2}}$ using either the backward difference or the Crank-Nicolson scheme. Values for ϕ^{n+1} are then computed in a similar manner using $F(\phi^{n+\frac{1}{2}})$ and the Crank-Nicolson scheme. Gourlay and Morris (Ref. 65) have also proposed implicit predictor-corrector techniques which can be applied to Eq. (20). In the conservative case ($F=1$), their technique is to define $\hat{G}(\phi)$ by the relation $G(\phi) = \phi\hat{G}(\phi)$ when such a definition exists, and to evaluate $\hat{G}(\phi^{n+1})$ using values for ϕ^{n+1} computed by an explicit predictor scheme. With $\hat{G}$ thereby known at the implicit time level, the equation can be treated as linear and corrected values of ϕ^{n+1} are computed by the Crank-Nicolson scheme.

A technique is described here for deriving linear implicit difference approximations for nonlinear differential equations. The technique is based on an expansion of nonlinear implicit terms about the solution at the known time level, t^n, and leads to a one-step two-level scheme which, being linear in unknown (implicit) quantities, can be solved efficiently without iteration. This idea was applied by Richtmyer and Morton (Ref. 66, p. 203) to a scalar nonlinear diffusion equation. Here, the technique is developed for problems governed by ℓ nonlinear equations in ℓ dependent variables which are functions of time and space coordinates. Although the present effort concentrates upon two spatial dimensions and time, the technique will be described for the three-dimensional, unsteady equations.

The solution domain is discretized by grid points having equal spacings in the computational coordinates, Δy^1, Δy^2 and Δy^3 in the y^1, y^2 and y^3 directions, respectively, and an arbitrary time step, Δt. The subscripts i, j, k and superscript n are grid point indices associated with y^1, y^2, y^3 and t, respectively, and thus $\phi^n_{i,j,k}$ denotes $\phi(y^1_i, y^2_j, y^3_k, t^n)$. It is assumed that the solution is known at the n level, t^n, and is desired at the (n+1) level, t^{n+1}. At the risk of an occasional ambiguity, one or more of the subscripts is frequently omitted, so that ϕ^n is equivalent to $\phi^n_{i,j,k}$.

The linearized difference approximation is derived from the following implicit time-difference replacement of Eq. (19):

$$(H^{n+1} - H^n)/\Delta t = \beta\left[\mathcal{D}(\phi^{n+1}) + S^{n+1}\right] + (1-\beta)\left[\mathcal{D}(\phi^n) + S^n\right] \tag{21}$$

where, for example, $H^{n+1} \equiv H(\phi^{n+1})$. The form of $\mathcal{D}$ and the spatial differencing are as yet unspecified. A parameter $(0 \le \beta \le 1)$ has been introduced so as to permit a variable centering of the scheme in time. Equation (21) produces a backward difference formulation for $\beta = 1$ and a Crank-Nicolson formulation for $\beta = \frac{1}{2}$.

The linearization is performed by a two-step process of expansion about the known time level t^n and subsequent approximation of the quantity $(\partial\phi/\partial t)^n \Delta t$, which arises from chain rule differentiation, by $(\phi^{n+1} - \phi^n)$. The result is

$$H^{n+1} = H^n + (\partial H/\partial \phi)^n (\phi^{n+1} - \phi^n) + O(\Delta t)^2 \tag{22a}$$

$$S^{n+1} = S^n + (\partial S/\partial \phi)^n (\phi^{n+1} - \phi^n) + O(\Delta t)^2 \tag{22b}$$

$$\mathcal{D}(\phi^{n+1}) = \mathcal{D}(\phi^n) + (\partial \mathcal{D}/\partial \phi)^n (\phi^{n+1} - \phi^n) + O(\Delta t)^2 \tag{22c}$$

The matrices $\partial H/\partial\phi$ and $\partial S/\partial\phi$ are standard Jacobians whose elements are defined, for example, by $(\partial H/\partial\phi)_{qr} \equiv \partial H_q/\partial\phi_r$. The operator elements of the matrix $\partial\mathcal{D}/\partial\phi$ are similarly ordered, i.e., $(\partial\mathcal{D}/\partial\phi)_{qr} \equiv \partial\mathcal{D}_q/\partial\phi_r$; however, the intended meaning of the operator elements requires some clarification. For the qth row, the operation $(\partial\mathcal{D}_q/\partial\phi)^n (\phi^{n+1} - \phi^n)$ is understood to mean that $\{\partial/\partial t\, \mathcal{D}_q[\phi(x,y,z,t)]\}^n \Delta t$ is computed and that all occurrences of $(\partial\phi_r/\partial t)^n$ arising from chain rule differentiation are replaced by

$(\phi_r^{n+1} - \phi_r^n)/\Delta t$.

After linearization as in Eqs. (22), Eq. (21) becomes the following linear implicit time-differenced scheme:

$$(\partial H/\partial\phi)^n(\phi^{n+1} - \phi^n)/\Delta t = \mathcal{D}(\phi^n) + S^n + \beta(\partial\mathcal{D}/\partial\phi + \partial S/\partial\phi)^n(\phi^{n+1} - \phi^n) \quad (23)$$

Although H^{n+1} is linearized to second order in Eq. (22a), the division by Δt in Eq. (21) introduces an error term of order Δt. A technique for maintaining formal second-order accuracy in the presence of nonlinear time derivatives is discussed by McDonald and Briley (Ref. 40), however, a three-level scheme results. Second-order temporal accuracy can also be obtained (for $\beta = \frac{1}{2}$) by a change in dependent variable to $\hat{\phi} \equiv H(\phi)$, provided this is convenient, since the nonlinear time derivative is then eliminated. The temporal accuracy is independent of the spatial accuracy.

On examination, it can be seen that Eq. (23) is linear in the quantity $(\phi^{n+1} - \phi^n)$ and that all other quantities are either known or evaluated at the n level. Computationally, it is convenient to solve Eq. (23) for $(\phi^{n+1} - \phi^n)$ rather than ϕ^{n+1}. This both simplifies Eq. (23) and reduces roundoff errors, since it is presumably better to compute a small $O(\Delta t)$ change in a $O(1)$ quantity than the quantity itself. To simplify the notation, a new dependent variable ψ defined by

$$\psi \equiv \phi - \phi^n \quad (24)$$

is introduced, and thus $\psi^{n+1} = \phi^{n+1} - \phi^n$, and $\psi^n = 0$. It is also convenient to rewrite Eq. (23) in the following simplified form:

$$(A + \Delta t\,\mathcal{L})\psi^{n+1} = \Delta t\left[\mathcal{D}(\phi^n) + S^n\right] \quad (25a)$$

where the following symbols have been introduced to simplify the notation:

$$A \equiv (\partial H/\partial\phi)^n - \beta\Delta t(\partial S/\partial\phi)^n \quad (25b)$$

$$\mathcal{L} \equiv -\beta(\partial\mathcal{D}/\partial\phi)^n \quad (25c)$$

It is noted that $\mathcal{L}(\psi)$ is a linear transformation and thus $\mathcal{L}(0) = 0$. Furthermore, if $\mathcal{D}(\phi)$ is linear, then $\mathcal{L}(\psi) = -\beta\mathcal{D}(\psi)$.

Spatial differencing of Eq. (25a) is accomplished simply by replacing derivative operators such as $\partial/\partial y^m$, $\partial^2/\partial y^m \partial y^m$ by corresponding finite difference operators, D_m, D_m^2. Henceforth, it is assumed that $\mathcal{D}$ and $\mathcal{L}$ have been discretized in this manner, unless otherwise noted.

Before proceeding, some general observations seem appropriate. The foregoing linearization technique assumes only Taylor expandability, an assumption already implicit in the use of a finite difference method. The governing equations and boundary conditions are addressed directly as a system of coupled nonlinear equations which collectively determine the solution. The approach thus seems more natural than that of making ad hoc linearization and decoupling approximations, as is often done in applying implicit schemes to coupled and/or nonlinear partial differential equations. With the present approach, it is not necessary to associate each governing equation and boundary condition with a particular dependent variable and then to identify various "nonlinear coefficients" and "coupling terms" which must then be treated by lagging, predictor-corrector techniques, or iteration. The Taylor expansion procedure is analogous to that used in the generalized Newton-Raphson or quasi-linearization methods for iterative solution of nonlinear systems by expansion about a known current guess of the solution (e.g., Bellman & Kalaba, Ref. 67). However, the concept of expanding about the previous time level apparently had not been employed to produce a noniterative implicit time-dependent scheme for coupled equations, wherein nonlinear terms are approximated to a level of accuracy commensurate with that of the time differencing. The linearization technique also permits the implicit treatment of coupled nonlinear boundary conditions, such as stagnation pressure and enthalpy at subsonic inlet boundaries, and in practice, this latter feature was found to be crucial to the stability of the overall method (Refs. 40 and 57).

Application of alternating-direction techniques. - Solution of Eq. (25a) is accomplished by application of an alternating-direction implicit (ADI) technique for parabolic-hyperbolic equations. The original ADI method was introduced by Peaceman and Rachford (Ref. 68) and Douglas (Ref. 69); however, the alternating-direction concept has since been expanded and generalized. A discussion of various alternating-direction techniques is given by Mitchell (Ref. 70) and Yanenko (Ref. 71).

The present technique is simply an application of the very general procedure developed by Douglas and Gunn (Ref. 60) for generating ADI schemes as perturbations of fundamental implicit difference schemes such as the backward-difference or Crank-Nicolson schemes.

For the present, it will be assumed that $\mathcal{D}(\phi)$ contains derivatives of first and second order with respect to y^1, y^2 and y^3, but no mixed derivatives. In this case, $\mathcal{D}$ can be split into three operators, $\mathcal{D}_1$, $\mathcal{D}_2$, $\mathcal{D}_3$ associated with the y^1, y^2 and y^3 coordinates and each having the functional form $\mathcal{D}_m = \mathcal{G}(\phi, \partial/\partial y^m, \partial^2/\partial y^m \partial y^m)$. Equation (25a) then becomes

$$\left[A+\Delta t(\mathcal{L}_1+\mathcal{L}_2+\mathcal{L}_3)\right]\psi^{n+1} = \Delta t\left[(\mathcal{D}_1+\mathcal{D}_2+\mathcal{D}_3)\phi^n + S^n\right] \tag{26}$$

Recalling that $\mathcal{L}(\psi^n) = 0$, the Douglas-Gunn representation of Eq. (26) can be written as the following three-step solution procedure:

$$(A+\Delta t\,\mathcal{L}_1)\psi^* = \Delta t\left[(\mathcal{D}_1+\mathcal{D}_2+\mathcal{D}_3)\phi^n + S^n\right] \tag{27a}$$

$$(A+\Delta t\,\mathcal{L}_2)\psi^{**} = A\psi^* \tag{27b}$$

$$(A+\Delta t\,\mathcal{L}_3)\psi^{n+1} = A\psi^{**} \tag{27c}$$

where ψ^* and ψ^{**} are intermediate solutions. It will be shown subsequently that each of Eqs. (27) can be written in narrow block-banded matrix form and solved by efficient block-elimination methods. If ψ^* and ψ^{**} are eliminated, Eqs. (27) become

$$(A+\Delta t\,\mathcal{L}_1)A^{-1}(A+\Delta t\,\mathcal{L}_2)A^{-1}(A+\Delta t\,\mathcal{L}_3)\psi^{n+1} = \Delta t\left[(\mathcal{D}_1+\mathcal{D}_2+\mathcal{D}_3)\phi^n + S^n\right] \tag{28}$$

If the multiplication on the left-hand side of Eq. (28) is performed, it becomes apparent that Eq. (28) approximates Eq. (26) to order $(\Delta t)^2$. Although the stability of Eqs. (27) has not been established in circumstances sufficiently general to encompass the Navier-Stokes equations, it is often suggested (e.g., Richtmyer & Morton, Ref. 66, p. 215) that the scheme is stable and accurate under conditions more general than those for which rigorous proofs are available. This latter notion was adopted here as a working hypothesis supported by favorable results obtained in actual computations (e.g., Refs. 40, 57-59).

A major attraction of the Douglas-Gunn scheme is that the intermediate solutions ψ^* and ψ^{**} are consistent approximations to ψ^{n+1}. Furthermore, for steady solutions, $\psi^n = \psi^* = \psi^{**} = \psi^{n+1}$ independent of Δt. Thus, physical boundary conditions for ψ^{n+1} can be used in the intermediate

steps without a serious loss in accuracy and with no loss for steady solutions. In this respect, the Douglas-Gunn scheme appears to have an advantage over locally one-dimensional (LOD) or "splitting" schemes, and other schemes whose intermediate steps do not satisfy the consistency condition. The lack of consistency in the intermediate steps complicates the treatment of boundary conditions and, according to Yanenko (Ref. 71, p. 33), does not permit the use of asymptotically large time steps. It is not clear that this advantage of the Douglas-Gunn scheme would always outweigh other benefits which might be derived from an alternative scheme. However, since the ADI scheme can be viewed as an approximate technique for solving the fundamental difference scheme, Eq. (25a), alternate techniques can readily be used within the present formulation.

It is worth noting that the operator $\mathcal{D}$ can be split into any number of components which need not be associated with a particular coordinate direction. As pointed out by Douglas and Gunn (Ref. 60), the criterion for identifying sub-operators is that the associated matrices be "easily solved" (i.e., narrow-banded). Thus, mixed derivatives can be treated implicitly within the ADI framework, although this would increase the number of intermediate steps and thereby complicate the solution procedure. Finally, only minor changes are introduced if, in the foregoing development of the numerical method, H, $\mathcal{D}$, and S are functions of the spatial coordinates and time, as well as ϕ.

Solution of the implicit difference equations. Since each of Eqs. (27) is implicit in only one coordinate direction, the solution procedure can be discussed with reference to a one-dimensional problem. For simplicity, it is sufficient to consider Eq. (27a) with $\mathcal{D}_2$, $\mathcal{D}_3 \equiv 0$. Consider the following three-point difference formulas:

$$D_m\phi \equiv \left[\alpha\Delta_- + (1-\alpha)\Delta_+\right]\phi/\Delta x_m = (\partial\phi/\partial x_m)_i + O\left[\Delta x_m^2 + (\alpha - 1/2)\Delta x_m\right] \quad (29a)$$

$$D_m^2\phi \equiv (\Delta_+\Delta_-)\phi/(\Delta x_m)^2 = (\partial^2\phi/\partial x_m^2)_i + O(\Delta x_m^2) \quad (29b)$$

for a typical computational coordinate x_m. Here, $\Delta_- \equiv \phi_i - \phi_{i-1}$, $\Delta_+ \equiv \phi_{i+1} - \phi_i$, and a parameter α has been introduced ($0 \le \alpha \le 1$) so as to permit continuous variation from backward to forward differences. The standard central difference formula is recovered for $\alpha = \frac{1}{2}$ and was used for all solutions reported here.

As an example, suppose that the qth component of the vector operator $\mathcal{D}_m$ has the form

$$\mathcal{D}_{mq}(\phi) = F_{1q}^T(\phi) \frac{\partial}{\partial x_m} G_{1q}(\phi) + F_{2q}^T(\phi) \frac{\partial^2}{\partial x_m^2} G_{2q}(\phi) \tag{30}$$

where F and G are column vector functions having the same (but an arbitrary number) of components; F^T denotes the transpose of F. The form of Eq. (30) permits governing equations having any number of first and second spatial derivative terms. Then,

$$\begin{aligned} \Delta t \frac{\partial \mathcal{D}_{mq}}{\partial t} \simeq \frac{\partial \mathcal{D}_{mq}}{\partial \phi} (\phi^{n+1} - \phi^n) \equiv \left[F_{1q}^T \frac{\partial}{\partial x_m} \frac{\partial G_{1q}}{\partial \phi} + \frac{\partial G_{1q}^T}{\partial x_m} \frac{\partial F_{1q}}{\partial \phi} \right]^n (\phi^{n+1} - \phi^n) \\ + \left[F_{2q}^T \frac{\partial^2}{\partial x_m^2} \frac{\partial G_{2q}}{\partial \phi} + \frac{\partial^2 G_{2q}^T}{\partial x_m^2} \frac{\partial F_{2q}}{\partial \phi} \right]^n (\phi^{n+1} - \phi^n) \end{aligned} \tag{31}$$

It is now possible to describe the solution procedure for Eq. (27a) for the one-dimensional case with $\mathcal{D}_m$ given by Eq. (30) and difference formulas given by Eq. (29). Because of the spatial difference operators, D_m and D_m^2, Eq. (27a) contains ψ_{i-1}^*, ψ_i^*, and ψ_{i+1}^*; consequently, the system of linear equations generated by writing Eq. (27a) at successive grid points $(x_m)_i$ can be written in block-tridiagonal form (simple tridiagonal for scalar equations, $\ell = 1$). The block-tridiagonal matrix structure emerges from rewriting Eq. (27a) as

$$a_i^n \psi_{i-1}^* + b_i^n \psi_i^* + c_i^n \psi_{i+1}^* = d_i^n \tag{32}$$

where a, b, c are square matrices and d is a column vector, each containing only n-level quantities. When applied at successive grid points, Eq. (32) generates a block-tridiagonal system of equations for ψ^* which, after appropriate treatment of boundary conditions, can be solved efficiently using standard block-elimination methods as discussed by Isaacson and Keller (Ref. 72, p. 58). The solution procedure for Eqs. (27b,c) is analogous to that just described for Eq. (27a). It is worth noting that the spatial difference parameter α can be varied with i or even term by term. For example, an "upwind difference" formula can be obtained if α is chosen as 1 or -1 depending on the sign of the elements of F_1; however, the formal accuracy of the method would then be reduced to first order.

Computing requirements. - Various block-elimination algorithms can be devised for solution of equations with block-banded matrix structures (cf., Isaacson & Keller, Ref. 72). Such algorithms can be derived using variants of Gaussian elimination for a banded matrix, but with the square submatrix elements of the banded matrix processed using matrix algebra. Thus, operations involving matrix subelements are not assumed to commute, and division by a matrix subelement is accomplished by computing the inverse and multiplying. Following this procedure, McDonald and Briley (Ref. 40) have developed an algorithm for block-tridiagonal systems arising from the second-order difference formulas, Eq. (29). The algorithm requires only one inverse per grid point. A standard operation count (scalar multiplications and divisions) has been performed for systems with L x L block elements and N diagonal block elements, i.e., L coupled equations along N grid points. The block-tridiagonal scheme requires $(3N-2)\ (L^3 + L^2)$ operations, the same as the matrix factorization scheme of Isaacson and Keller (Ref. 72). Assuming there are N grid points in each coordinate direction, the total number of operations for a single time step is obtained from the operation count for solution of one block-banded system by multiplying by 2N and $3N^2$ for two and three dimensions, respectively.

For comparison, it is noted that in the case of the Navier-Stokes equations, merely evaluating the right-hand side of Eq. (27a), which would be a minimum requirement for a one-step explicit scheme, requires 302 N operations for a 3-point difference formula.

In view of the many factors involved, it is difficult to evaluate precisely or with any generality the overall computational efficiency of the MINT method relative to various other methods. However, the foregoing operational counts show that the effort expended to solve the implicit difference equations by block-elimination is not excessive compared with that necessary simply to evaluate the differenced Navier-Stokes equations, let alone the various other bookkeeping tasks present in most large-scale computer programs for fluid dynamics problems. In the solutions presented here, the solution of the block-tridiagonal systems using double precision arithmetic required only about twenty percent of the total computer time per time step.

Artificial dissipation. - In computing solutions for high Reynolds number flows, it is often necessary to add a form of artificial viscosity or dissipation. Artificial dissipation in some form is often useful in practical calculations to stabilize the overall method when function boundary conditions are applied, when coarse mesh spacing is used, or in the presence of discontinuities. The need for artificial dissipation arises in certain instances when centered spatial difference approximations are used for first

derivative terms. The use of artificial dissipation is thus a matter of spatial differencing technique, and it is commonly employed in either explicit or inherent form, and in both explicit and implicit difference schemes.

One possible dissipation term in common use is based on an observation (e.g., Roache, Ref. 73, p. 162) that for a linear model problem representing a one-dimensional balance of convection and diffusion terms, solutions obtained using central differences for the convection term are well behaved provided the mesh Reynolds number $Re_{\Delta x_m} = |u_m| \Delta x_m Re$ is ≤ 2, but that qualitative inaccuracies (associated with boundary conditions) occur for $Re_{\Delta x_m} > 2$. This suggests the use of an artificial viscosity term of the form $\epsilon_m D_m^2 \phi$, where

$$\epsilon_m = \begin{cases} \dfrac{|u_m| \Delta x_m}{2} - \dfrac{1}{Re} = \dfrac{1}{Re}\left(\dfrac{Re_{\Delta x_m}}{2} - 1\right) & Re_{\Delta x_m} > 2 \\ 0 & Re_{\Delta x_m} \leq 2 \end{cases} \tag{33}$$

to ensure that the local effective mesh Reynolds number is no greater than two. The simplified analysis presented here was extended for the generalized tensor equations presented previously and the resulting dissipation terms were added to the continuity and momentum equations.

A second type of artificial damping which is a fourth-order dissipation term has been suggested by Beam and Warming (Ref. 39) to damp small wavelength disturbances. In the present formulation an explicit fourth-order damping term was added directly to the fundamental difference scheme, Eq. (25a), as follows:

$$(A + \Delta t \mathcal{L}) \psi^{n+1} = \Delta t \left[\mathcal{D}(\phi^n) + S^n\right] + \sum_{m=1}^{3} (\Delta x_m)^4 \frac{\omega_m}{8} \frac{\partial^4 \phi^n}{\partial x_m^4} \tag{34}$$

Note that the dissipative coefficients ω_m implicitly contain the time step Δt; however, since the dissipation term is treated explicitly (to retain the block tridiagonal matrix structure), a linear von Neumann stability analysis shows that the coefficients ω_m must be in the range of $0 \leq \omega_m \leq 1$ for stability (Ref. 39). This condition actually implies a limit on the maximum permissible time step which may be taken, however, in the present formulation this was not a restriction. The advantage of the fourth-

derivative dissipation added in Eq. (34) over the more conventional artificial viscosity formulation, Eq. (33), is that the formal accuracy of the method is not altered, whereas Eq. (33) reduces the formal accuracy to first order when $Re_{\Delta x_m} > 2$. Strictly speaking, the overall method is second-order accurate since $Re_{\Delta x_m} \to 0$ as the mesh is refined. It should be remembered, however, that such asymptotic truncation error estimates are meaningful only for sufficiently small mesh size; whereas in practical calculations of complex flows mesh resolution capabilities are almost always strained.

RESULTS

Solution of the Heat Conduction Equation

Solutions of the heat conduction equation were the first test cases of the MINT code applied in its general tensor form. In vector notation the equation is given by

$$\nabla^2 \phi = \partial \phi / \partial t \tag{35}$$

which can be expressed in tensor form as

$$\frac{1}{\sqrt{g}} \frac{\partial}{\partial y^i} \left(g^{ij} \frac{\partial \phi}{\partial y^i} \sqrt{g} \right) = \partial \phi / \partial t \tag{36}$$

(36) y^i represents the i^{th} general coordinate and g_{ij} are the coefficients of the metric tensor. It should be noted that Eq. (36) is not a trivial test case in as much as the equation contains both metric coefficients and their derivatives.

Two cases were considered. In both cases the solution domain was the region interior to the closed curve formed by an elliptical arc, the x-axis and an arc generated by points with an equal normal distance from the elliptical arc. An illustration is shown in Fig. 2. In both cases the coordinate system was generated by the two arcs consisting of the elliptical arc and the outer arc. The elliptical arc was given as raw geometric data and then fit with a parametric curve developed in a piecewise fashion. The fitting process used least squares so that eventually, measured data could be used. The parameterization for the outer arc was taken as its arc length; for the elliptical arc, it was imposed from the outer arc under the condition that lines joining points of like parameter values are normal to each arc. Given this parameterization, the coordinate transformation is given in Eq. (14).

In the first test case initial conditions were specified such that all boundary points were equal to zero and all interior points were equal to unity. The zero values on the boundary were held as boundary conditions. The solution then decayed to zero throughout the domain as the equation was marched in time. In the second case zero derivative conditions were applied at the inner and outer curved boundaries. The segments of the x-axis were set at zero and unity, respectively. Initially all interior points

were set to unity and the solution was then allowed to develop in time. At large times the solution satisfied the condition $\nabla^2\phi = 0$ as it should. These solutions of the heat conduction equation do not represent as stringent a test of the coordinate system as would a solution of the Navier-Stokes equations. However, the heat conduction equation is not trivial and the solutions obtained demonstrate the potential of the current coordinate system. A feature of this system is that it does not require analytically specified curves as boundaries. Solutions of the Navier-Stokes equations also were attempted in this same coordinate system which was generated from raw geometric data; however, in this case successful solutions were not obtained.

The source of the difficulty in the Navier-Stokes case was the appearance of second derivatives of the metric coefficients. In contrast the heat conduction equation only contained first derivatives of the metric coefficients. When the boundary was expressed as a non-analytically specified curve, first derivatives of the metric coefficients were sufficiently smooth to obtain reasonable solutions, however, second derivatives were not.

Present efforts now are aimed at resolving this problem; two approaches are being taken. In the first approach the equations are being reformulated in a manner which does not require second derivatives of the metric coefficients. In the second approach the curve fitting routines are being refined further so as to produce sufficiently smooth derivatives to allow a Navier-Stokes solution.

Flow About a Circular Cylinder

The first Navier-Stokes solution calculated under the present effort was the flow about a circular cylinder at Reynolds number (based upon diameter) equal to forty. This case was chosen since it represents a relatively simple geometry and since both experimental data and other solutions were available for comparison. A comprehensive list of references on both experimental work and numerical calculations is given by Ref. 30.

The dependent variables used for this calculation were the density and the contravariant components of the velocity, v^1 and v^2. The calculation was initiated by specifying the inviscid solution throughout the flow field and then imposing a zero velocity condition on wall boundary points. The velocity was set equal to zero and the inviscid transverse momentum equation ($\partial p/\partial n = 0$) was solved at the cylinder surface. The latter boundary condition is required to determine a value of density at the wall grid point and, in the present case of constant total temperature, this condition is

equivalent to $\partial\rho/\partial n = 0$. It should be noted that the condition of constant total temperature and zero slip velocity implies $\partial T/\partial n = 0$ at the wall. At the outer boundary, velocity and density were set to their inviscid values over the upstream three quarters of the outer boundary ($0 \leq \theta \leq 3\pi/4$). First derivatives of the physical velocity components were set to zero and the pressure was set to its inviscid value over the remainder of the far field boundary. The far field boundary was taken to be fifteen diameters from the cylinder center (A = 29). In this computation the only artificial viscosity term added was that based on the mesh Reynolds number criterion, Eq. (33). The present predictions were obtained with a 35 x 35 mesh (including boundary points), and the coordinate system employed is shown in Figs. (3a,b). A special case of Eq. (16) is the Roberts boundary layer transformation (Ref. 78) which is obtained by setting m = 0. With a damping factor D = 2.7, this transformation was used to concentrate grid points both near the wall and near the front and rear stagnation points as shown in Fig. 3. The loopwise distribution was computed by a rigid translation of Eq. (16) with m = 0. The result was the distribution $\theta(\theta) = \tanh(2\theta D/\pi - D)/\tanh D$ where D = 1.5. The computation time for the present nonorthogonal form of the governing equations, Eqs. (7, 9-13), is approximately 5.9×10^{-4} CPU minutes per grid point per time step on the UNIVAC 1110, and approximately 80 time steps were required to obtain the steady state solution.

The present prediction of the surface pressure along with predictions of Son and Hanratty (Ref. 74) and Kawaguti (Ref. 75) are shown in Fig. 4. The Kawaguti pressure prediction was given relative to the predicted rear stagnation point pressure and in this figure the Kawaguti rear stagnation point pressure was arbitrarily set at the Son and Hanratty value. The predictions of Refs. 74 and 75 both were obtained from solutions of the incompressible Navier-Stokes equations. The present solution is obtained from the compressible equations at a Mach number equal to 0.2. As shown in Fig. 4 all three solutions are in reasonable agreement with each other. The discrepancies may be due to the different numerical methods or the effect of compressibility. Another possible source of discrepancy in the leading edge region is the application of the inviscid transverse momentum equation as a wall boundary condition in the present formulation. An improved wall boundary condition is probably required for proper representation of both the leading edge stagnation region and separated flow regions. It is believed that a one-sided difference representation of the normal momentum equation at the wall is a more realistic boundary condition, since this boundary condition allows a normal pressure gradient consistent with the momentum balance in the near wall region. The centerline velocity prediction is compared to the data of Coutanceau and Bouard (Ref. 30) and the predictions of Kawaguti (Ref. 75), Apelt (Ref. 76) and Nieuwstadt

and Keller (Ref. 77) in Fig. 5. Again the agreement between data and all analyses is good. Predicted streamline locations are shown in Fig. 6 and streamwise velocity profiles at several azimuthal locations are shown in Fig. 7. A comparison of Figs. 5 and 6 shows a discrepancy in the wake length, however, this discrepancy represents less than one half the radial grid spacing at the near wake closure point. The values of the wake length given by other authors (Refs. 30, 75, 76, 77) are higher than the present prediction, however, the present results were obtained with a relatively coarse mesh. Also, use of the contravariant velocity components, which was subsequently abandoned in the airfoil computations, is believed to increase the truncation error in the numerical predictions.

Flow About a Joukowski Airfoil

The second Navier-Stokes solution calculated was the flow about an 11 percent thick Joukowski airfoil at zero angle of attack and a Reynolds number of eighty (80) based on the airfoil chord length. The case represents a much more severe test of the MINT tensor code because of the significant variation in the metric tensor coefficients throughout the computational field. The coordinate systems for the Joukowski airfoil computations presented herein were obtained using the analytic Joukowski transformation in conjunction with Eq. (16) (for $m = 0$ and $D = 3.3$) in the pseudoradial coordinate direction. No redistribution of mesh points in the aximuthal (loopwise) direction was required for the calculations presented. The Joukowski airfoil results at $Re = 80$ were obtained using a 41 x 22 mesh (including boundary points) with the far field boundary taken to be approximately fifteen chord lengths from the airfoil. The coordinate system employed is shown in Figs. (8a,b).

The dependent variables employed in this calculation were the density and the physical velocity components, u_1 and u_2. The calculation was initiated by specifying the inviscid solution throughout the flow field and then imposing a zero velocity condition on wall boundary points. The velocity was set equal to zero and the inviscid transverse momentum equation ($\partial p/\partial n = 0$) was solved at the airfoil surface. At the outer boundary, velocity and density were set to their inviscid values over the upstream three quarters of the outer boundary. First derivatives of the velocity components were set to zero and the pressure was set to its inviscid value over the remainder of the far field boundary. In this computation, both the fourth-order damping, (Eq. 34), and the artificial viscosity term based on the mesh Reynolds number criterion, (Eq. 33), were added to the governing

equations, because it was found that the conventional dissipation term alone (Eq. 33) did not prevent spatial oscillations from occurring. The relatively coarse grid employed in the pseudo-radial direction (22 points) led to some difficulties at the far field boundaries where the velocity components were specified. Specifically, the computed velocities near the boundary did not approach the inviscid values as uniformly as desired.

The predicted airfoil surface pressure distribution is shown in Fig. 9 and computed streamline locations are shown in Fig. 10. The computed streamwise and transverse velocity profiles are shown in Figs. 11 and 12, respectively, at the azimuthal locations defined by the nondimensional surface arc length coordinate, $s_1/s_{1_{max}}$ (see Fig. 8). The computed centerline velocity profile downstream of the trailing edge is shown in Fig. 13. These predictions generally exhibit qualitatively reasonable behavior, except in the vicinity of the airfoil leading edge where the pressure seems to be somewhat higher than expected. This behavior might be attributable to the application wall boundary condition $\partial p/\partial n = 0$, which is physically incorrect in the leading edge region.

Finally, the Navier-Stokes calculation for the flow about an 11 percent thick Joukowski airfoil at zero angle of attack and a Reynolds number of 1000 was initiated to demonstrate the high Reynolds number capability of the MINT code. The Joukowski airfoil results at $Re_\ell = 1000$ were obtained using a 41 x 30 mesh (including boundary points) with the far field boundary taken to be approximately ten chord lengths from the airfoil. The coordinate system employed is similar to that shown in Fig. 8, but with a higher concentration of grid points near the airfoil surface. This calculation was begun by applying approximate boundary layer corrections to the inviscid velocity field. Again the velocity was set equal to zero and the inviscid transverse momentum equation ($\partial p/\partial n = 0$) was solved at the airfoil surface. This calculation was not run to convergence because of time and funding constraints. The surface pressure prediction is shown in Fig. 14, the streamline pattern is shown in Fig. 15 and the computed streamwise velocity profiles at several azimuthal locations are shown in Fig. 16 for this case. Again, these results appear to be qualitatively reasonable although the flow over the airfoil surface had not yet separated at the time of these plots.

CONCLUSIONS

Two major areas have been investigated under the present effort. The first area concentrates upon the development of a coordinate system for calculating the flow about an isolated airfoil. The second area concentrates upon the flow field calculation itself.

A fundamental requirement for any airfoil flow calculation procedure is the generation of an efficient and accurate system of coordinates. The efficiency is needed if eventual applications to three-dimensional and/or time-dependent geometries are contemplated; the accuracy is needed to insure the fundamental integrity of the overall algorithm and to control its error growth.

Under the present effort the process of coordinate generation for the entire class of airfoil geometries has progressed in an orderly fashion leading to a solution of the heat conduction equation in a coordinate system generated from a discrete specification of boundary points. The major problem preventing a solution of the Navier-Stokes equations with this coordinate generation procedure appears to be a lack of smoothness in the higher derivatives of the metric coefficients. Under investigation are both an alternate form of the Navier-Stokes equations requiring less smoothness in metric data and a new coordinate generating technique with stronger smoothness properties.

The second portion of the current effort has successfully solved the Navier-Stokes equations about isolated bodies. Predictions for low Reynolds number flow about a cylinder are in good agreement with both experimental data and other numerical predictions. Calculations of the flow field about a Joukowski airfoil at $Re_\ell = 80$ are qualitatively reasonable; at $Re_\ell = 1000$ no adverse high Reynolds number effects are observed.

Several problems which have arisen in the course of the present effort require further work. These include a thorough investigation of both wall and far field boundary conditions. As mentioned previously a one-sided difference representation of the normal momentum equation at the wall should be considered as a boundary condition for determining the wall value of density. In the far field, solution of the Euler equations over a portion of the outer computational boundary may alleviate the numerical difficulties encountered in that region of the flow field, without resorting to mesh refinement in the inviscid portion of the flow field.

REFERENCES

1. Geising, J. P. : Nonlinear Two Dimensional Potential Flow with Lift. Journal of Aircraft, Vol. 5, No. 2, March-April 1968, pp. 135-143.

2. Geising, J. P., Kalman, T. P. and Rodden, W. P.: Subsonic Steady and Oscillatory Aerodynamics for Multiple Interfering Wings and Bodies. Journal of Aircraft, Vol. 9, No. 10, October 1972, pp. 693-702.

3. Bauer, F., Garabedian, P. and Korn, D.: A Theory of Supercritical Wing Sections with Computer Programs and Examples. Lecture Notes in Economics and Mathematical Systems, Vol. 66, Springer-Verlag, Berlin, 1972.

4. McDonald, H. and Fish, R. W.: Practical Calculations of Transitional Boundary Layers. International Journal of Heat and Mass Transfer, Vol. 16, No. 9, 1973, pp. 1729-1744.

5. Kreskovsky, J. P., Shamroth, S. J., and McDonald, H.: Application of a General Boundary Layer Analysis to Turbulent Boundary Layers Subjected to Strong Favorable Pressure Gradients. Journal of Fluids Engineering, Vol. 97, No. 3, June 1975, pp. 217-224.

6. Nash, J. F. and Patel, V. C.: Calculations of Unsteady Turbulent Boundary Layers with Flow Reversal. NASA CR-2546, May 1975.

7. Briley, W. R. and McDonald, H.: Numerical Prediction of Incompressible Separation Bubbles. Journal of Fluid Mechanics, Vol. 69, Part 4, 1975, pp. 631-656.

8. Shamroth, S. J. and Kreskovsky, J. P.: A Weak Interaction Study of the Viscous Flow about Oscillating Airfoils. NASA CR-132425, May 1974.

9. Kreskovsky, J. P., Shamroth, S. J. and Briley, W. R.: A Numerical Study of the Unsteady Leading Edge Separation Bubble on an Oscillating Airfoil. Computer Methods in Applied Mechanics and Engineering, Vol. 11, No. 1, April 1977, pp. 39-56.

10. McCullough, G. B. and Gault, D. E.: Examples of Three Representative Types of Section Stall at Low Speed. NACA TN 2502, September 1951.

11. Liiva, J.: Unsteady Aerodynamic and Stall Effects on Helicopter Rotor Blade Airfoil Sections. Journal of Aircraft, Vol. 6, No. 1, January 1969, pp. 46-51.

REFERENCES (CONT'D)

12. Velkoff, H. R., Blaser, D. A. and Jones, K. M.: Boundary Layer Discontinuity on a Helicopter Rotor Blade in Hovering. Journal of Aircraft, Vol. 8, 1971, pp. 101-107.

13. Isogai, K.: An Experimental Study of the Unsteady Behavior of an Airfoil During Dynamic Stall with Special Reference to the Mechanism of the Stall Overshoot Effect. MIT ASRL TR-130-2, June 1970.

14. McCroskey, W. J. and Philippe, J. J.: Unsteady Viscous Flow on Oscillating Airfoils. AIAA Paper 74-182, 1974.

15. McCroskey, W. J., Carr, L. W., and McAlister, K. W.: Dynamic Stall Experiments on Oscillating Airfoils. AIAA Journal, Vol. 14, No. 1, January 1976, pp. 57-63.

16. Parker, A. G.: Force and Pressure Measurements on an Airfoil Oscillating through Stall. Journal of Aircraft, Vol. 13, No. 10, October 1976, pp. 823-827.

17. Landgrebe, A. J. and Bellinger, E. D.: A Systematic Study of Helicopter Rotor Stall Using Model Rotors. American Helicopter Society Preprint 804, 1974.

18. McCroskey, W. J.: Recent Developments in Dynamic Stall. Symposium on Unsteady Aerodynamics, Kinney, R. B. ed., University of Arizona, Tucson, 1975, pp. 1-23.

19. Ham, N. D. and Garelick, M. S.: Dynamic Stall Considerations in Helicopter Rotors. Journal of the American Helicopter Society, Vol. 13, No. 2, April 1968, pp. 49-55.

20. Ham, N. D.: Aerodynamic Loading on a Two Dimensional Airfoil During Dynamic Stall. AIAA Journal, Vol. 6, No. 10, October 1968, pp. 1927-1934.

21. Baudu, N., Sagner, M. and Souquet, J.: Modelisation du Decrochage Dynamique d'un Profil Oscillant. AAAF 10th Colluque d'Aerodynamique Appliquee, Lille, France, November 1973.

22. Ericsson, L. E. and Reding, J. P.: Dynamic Stall Analysis in Light of Recent Numerical and Experimental Results. AIAA Preprint No. 75-26, 1975.

REFERENCES (CONT'D)

23. Ericsson, L. E. and Reding, J. P.: Spilled Leading Edge Vortex Effects on Dynamic Stall Characteristics. Journal of Aircraft, Vol. 13, No. 4, April 1976, pp. 313-315.

24. Lang, J. D.: A Model for the Dynamics of a Separation Bubble Used to Analyze Control-Surface Buzz and Dynamic Stall. AIAA Paper 75-867, 1975.

25. Carta, F. O., Commerford, G. L. and Carlson, R. G.: Determination of Airfoil and Rotor Blade Dynamic Stall Response. Journal of the American Helicopter Society, Vol. 18, No. 2, 1973, pp. 31-39.

26. Scruggs, R. M., Nash, J. F. and Singleton, R. E.: Analysis of Flow Reversal Delay for a Pitching Airfoil. AIAA Paper No. 74-183, 1974.

27. Crimi, P. and Reeves, B. L.: A Method for Analyzing Dynamic Stall of Helicopter Rotor Blades. NASA CR-2009, May 1972.

28. Gregory, N. and O'Reilly, C. L.: Low Speed Aerodynamic Characteristics of NACA 0012 Airfoil Section, Including the Effects of Upper Surface Roughness Simulating Hoarfrost. Aero Report 1308, National Physics Laboratory, 1970.

29. Ridder, S. O.: Experimental Studies of the Leading Edge Suction Force, Including the Maximum Attainable Suction Force Versus Reynolds Number and the Induced Distributions on Various Wing Planforms and Air Intakes. Ninth ICAS Congress Paper No. 74-47, Haifa, 1974.

30. Coutanceau, M. and Bouard, R.: Experimental Determination of the Main Features of the Viscous Flow in the Wake of a Circular Cylinder in Uniform Translation. Part 1. Steady Flow. Journal of Fluid Mechanics, Vol. 79, 1977, pp. 231-236.

31. Mehta, U. B. and Lavan, Z.: Starting Vortex, Separation Bubble and Stall: A Numerical Study of Laminar Unsteady Flow About an Airfoil. Journal of Fluid Mechanics, Vol. 67, 1975, pp. 227-256.

32. Wu, J. C. and Sampath, S.: A Numerical Study of Viscous Flow About an Airfoil. AIAA Paper 76-337, 1976.

33. Wu, J. C. and Thompson, J. F.: Numerical Solutions of Time-Dependent Incompressible Navier-Stokes Equations Using an Integro-Differential Formulation. Computers and Fluids, Vol. 1, 1973, pp. 197-215.

34. Verhoff, A.: Numerical Solution of Subsonic Viscous Inviscid Interacting Flows. AFFDL-TR-76-64, July 1976.

35. MacCormack, R. W.: The Effect of Viscosity in Hypervelocity Impact Cratering. AIAA Paper No. 69-354, 1967.

36. MacCormack, R. W.: An Efficient Numerical Method for Solving the Time-Dependent Compressible Navier-Stokes Equations at High Reynolds Number. NASA TM X-73129, July 1976.

37. Steger, J. L.: Implicit Finite Difference Simulation of Flow About Arbitrary Geometries with Application to Airfoils. AIAA Paper 77-665, 1977.

38. Thompson, J. F., Thames, F. C. and Mastin, C. M.: Automatic Numerical Generation of Body Fitted Curvilinear Coordinate System for Field Containing Any Number of Arbitrary Two-Dimensional Bodies. Journal of Computational Physics, Vol. 15, 1974, pp. 299-319.

39. Beam, R. and Warming, R. F.: An Implicit Finite Difference Algorithm for Hyperbolic Systems in Conservation-Law-Form. Journal of Computational Physics, Vol. 22, September 1976, pp. 87-110.

40. Briley, W. R. and McDonald, H.: An Implicit Numerical Method for the Multidimensional Compressible Navier-Stokes Equations. United Aircraft Research Laboratories Report M911363-6, 1973.

41. Lindemuth, I. and Killeen, J.: Alternating Direction Implicit Techniques for Two-Dimensional Magnetohydrodynamic Calculations. Journal of Computational Physics, Vol. 13, 1973, pp. 181-208.

42. Eiseman, P. R.: A Coordinate System for a Viscous Transonic Cascade Analysis. Journal of Computational Physics, accepted for 1978 publication.

43. Eiseman, P. R., McDonald, H., and Briley, W. R.: A Method for Computing Three-Dimensional Viscous Diffuser Flows. United Technologies Research Center Report, R75-911737-1, July 1975.

44. Theodorsen, T., and Garrick, I. E.: General Potential Theory of Arbitrary Wing Sections. NACA TR No. 452, 1933.

45. Ives, D. C.: A Modern Look at Conformal Mapping, Including Multiply Connected Regions. AIAA Journal, Vol. 14, No. 8, August 1976, pp. 1006-1011.

46. Ives, D. C. and J. F. Livtermoza: Analysis of Transonic Cascade Flow Using Conformal Mapping and Relaxation Techniques. AIAA Paper No. 76-370, 9th Fluid and Plasma Dynamics Conference, 1976.

47. Henrici, P.: Applied and Computational Complex Analysis Vol. 1. John Wiley and Sons, New York, 1974.

48. Gunning, R. C., and Rossi, H.: Several Complex Variables. Prentice Hall, Inc., Englewood Cliffs, New Jersey, 1965.

49. Bishop, R. L. and Crittenden, R. J.: Geometry of Manifolds. Academic Press, Inc., New York, 1964.

50. McVittie, G. C.: A Systematic Treatment of Moving Axes in Hydrodynamics. Proceedings of the Royal Society A, 196, pp. 285-300.

51. McVittie, G. C.: General Relativity and Cosmology. The University of Illinois Press, Urbana, Ill., 1965.

52. Walkden, F.: The Equations of Motion of a Viscous, Compressible Gas Referred to an Arbitrarily Moving Coordinate System. Royal Aircraft Establishment, Technical Report No. 66140, April 1966.

53. Misner, C. W., Thorne, K. S., and Wheeler, J. A.: Gravitation. W. H. Freeman and Co., San Francisco, 1973.

54. Landau, L. D. and Lifshitz, E. M.: Fluid Mechanics. Addison-Wesley, Paris, 1959.

55. Eiseman, P. R.: The Numerical Solution of the Fluid Dynamical Equations in Curvilinear Coordinates. Air Force Weapons Laboratory Report AFWL-TR-73-172, 1973.

56. Lawson, C. L. and Hanson, R. J.: Solving Least Squares Problems. Prentice-Hall, New York, 1974.

57. Briley, W. R., McDonald, H., and Gibeling, H. J.: Solution of the Multidimensional Compressible Navier-Stokes Equations by a Generalized Implicit Method. United Technologies Research Center Report R75-911363-15, January 1976.

58. Gibeling, H. J., McDonald, H. and Briley, W. R.: Development of a Three-Dimensional Combustor Flow Analysis, Vols. I and II: Theoretical Studies. Air Force Aero Propulsion Laboratory Report AFAPL-TR-75-59; Vol. I, July 1975; Vol. II, October 1976.

59. Levy, R., Shamroth, S. J., Gibeling, H. J., and McDonald, H.: A Study of the Turbulent Shock Wave Boundary Layer Interaction. Air Force Flight Dynamics Laboratory Report AFFDL-TR-76-163, February 1977.

60. Douglas, J. and Gunn, J. E.: A General Formulation of Alternating Direction Methods. Numerische Math., Vol. 6, 1964, pp. 428-453.

61. Chorin, A. J.: Numerical Study of Thermal Convection in a Fluid Layer Heated from Below. AEC R&D Report TID-4500 (also New York Univ. Report NYO-1480-61), 1966.

62. Ames, W. F.: Numerical Methods for Partial Differential Equations. Barnes & Noble, Inc., New York, 1969.

63. von Rosenburg, D. A.: Methods for the Numerical Solution of Partial Differential Equations. American Elsevier Publishing Co., Inc., New York, 1969.

64. Douglas, J. and Jones, B. F.: On Predictor-Corrector Methods for Nonlinear Parabolic Differential Equations. Soc. for Indust. Appl. Math., Vol. 11, 1963, pp. 195-204.

65. Gourlay, A. R. and Morris, J. L.: Finite-Difference Methods for Nonlinear Hyperbolic Systems. Math. Comp., Vol. 22, 1968, pp. 28-39.

66. Richtmyer, R. D. and Morton, K. W.: Difference Methods for Initial Value Problems. Second Edition. Interscience Publishers, New York, 1967.

67. Bellman, R. E. and Kalaba, R. E.: Quasilinearization and Nonlinear Boundary-Value Problems. American Elsevier Publ. Co., Inc., New York, 1965.

68. Peaceman, D. W. and Rachford, H. H.: The Numerical Solution of Parabolic and Elliptic Differential Equations. Soc. for Indust. Appl. Math., Vol. 3, 1955, pp. 28-41.

69. Douglas, J.: On the Numerical Integration of $u_{xx} + u_{yy} = u_t$ by Implicit Methods. Soc. for Indust. Appl. Math., Vol. 3, 1955, pp. 42-65.

70. Mitchell, A. R.: Computational Methods in Partial Differential Equations. John Wiley & Sons, Inc., New York, 1969.

71. Yanenko, N. N.: The Method of Fractional Steps, Translation Edited by M. Holt. Springer-Verlag, New York, 1971.

72. Isaacson, E. and Keller, H. B.: Analysis of Numerical Methods. John Wiley & Sons, Inc., New York, 1966.

73. Roache, P. J.: Computational Fluid Dynamics. Hermosa Publisher, Albuquerque, New Mexico, 1972.

74. Son, J. S. and Hanratty, T. J.: Numerical Solution for the Flow Around a Circular Cylinder at Reynolds Numbers of 40, 200 and 500. Journal of Fluid Mechanics, Vol. 35, 1969, pp. 369-386.

75. Kawaguti, M.: Numerical Solution of the Navier-Stokes Equations for the Flow Around a Circular Cylinder at Reynolds Number 40. Journal of the Physical Society of Japan, Vol. 8, 1953, pp. 747-757.

76. Apelt, C. J.: The Steady Flow of a Viscous Fluid Past a Circular Cylinder at Reynolds Numbers of 40 and 44. Aeronautical Research Council R. & M. No. 3175, 1958.

77. Nieuwstadt, F. and Keller, H. B.: Viscous Flow Past Circular Cylinders. Computers and Fluids, Vol. 1, 1973, pp. 59-71.

78. Roberts, G. O.: Computational Meshes for Boundary Layer Problems. Proceedings of the Second International Conference on Numerical Methods in Fluid Dynamics, Springer-Verlag, New York, 1971, p. 171.

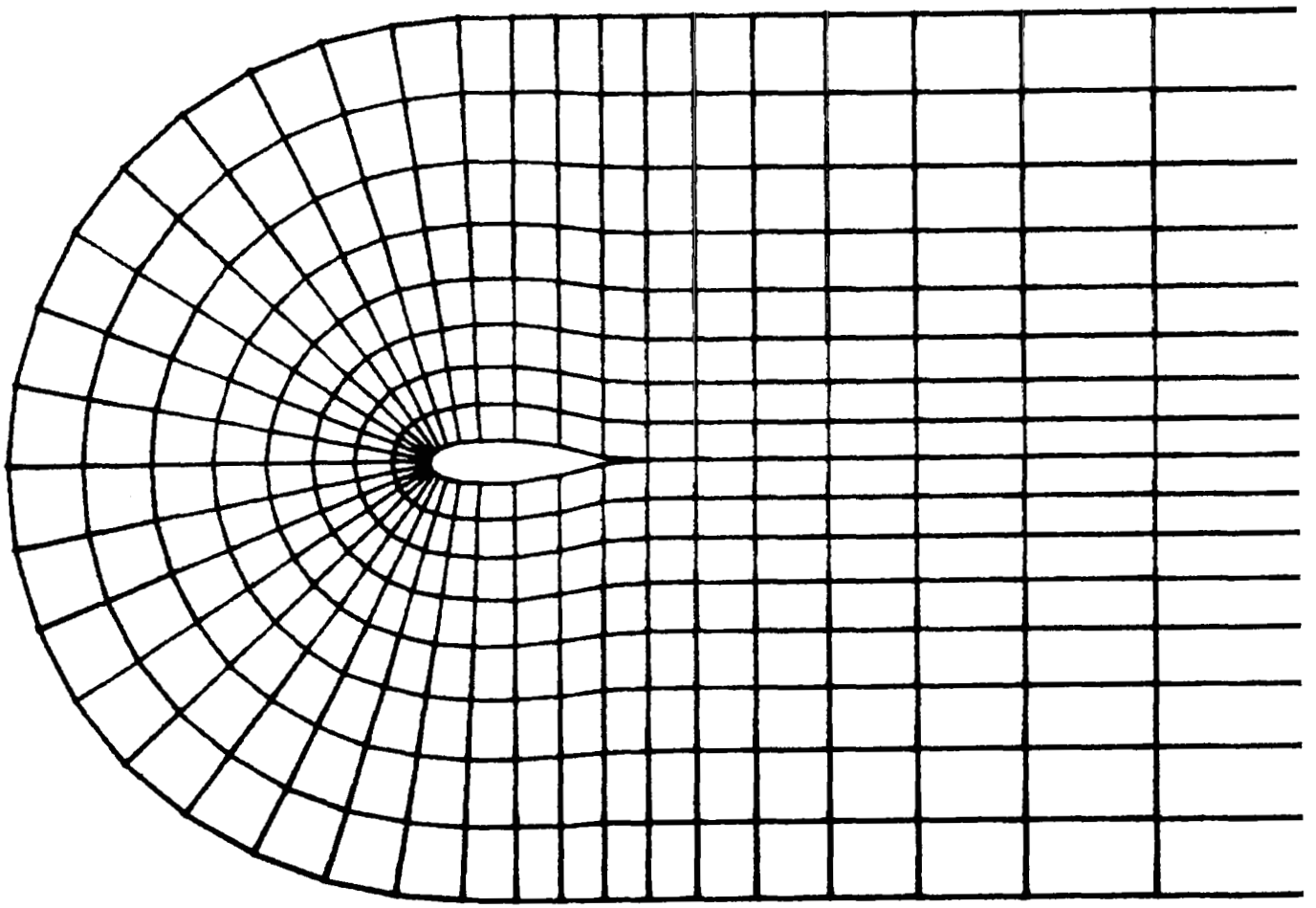

Figure 1.—A coordinate system for flows with a narrow wake.

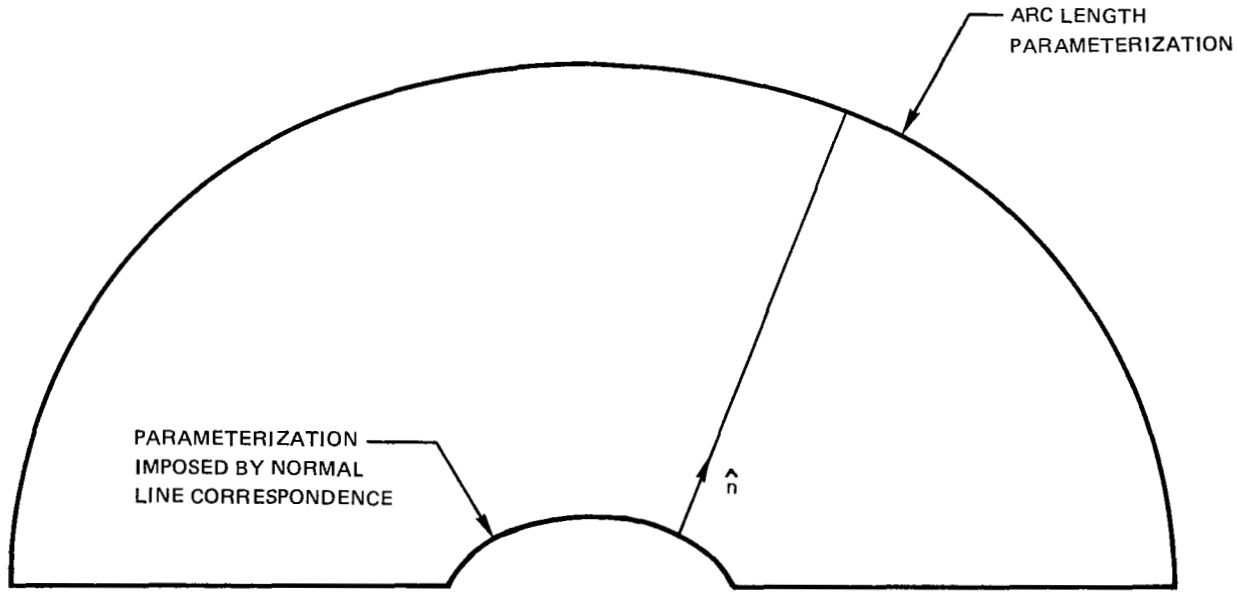

Figure 2. — Computational domain for test problems with the heat equation.

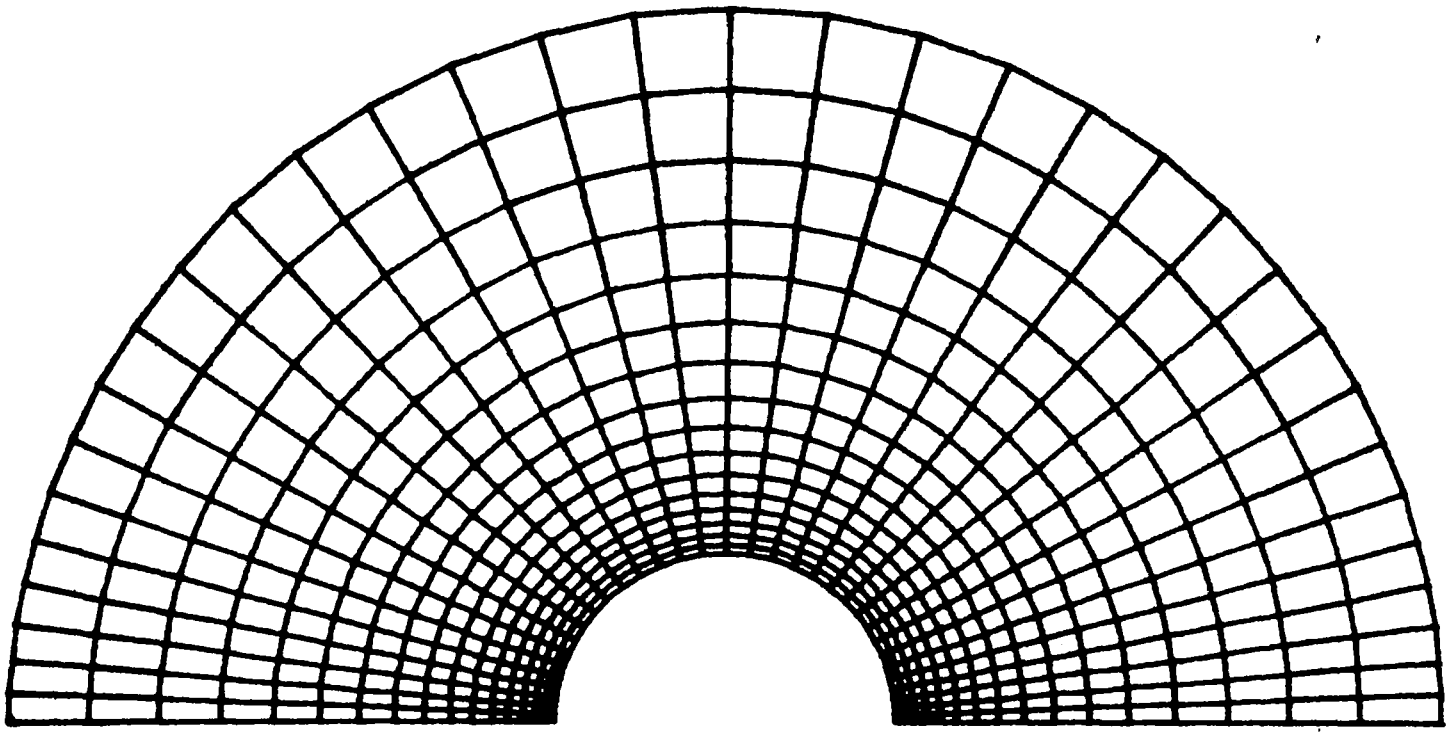

Figure 3a. - Circular cylinder coordinate system, $Re_D = 40$; near field (radial locations 1 through 17).

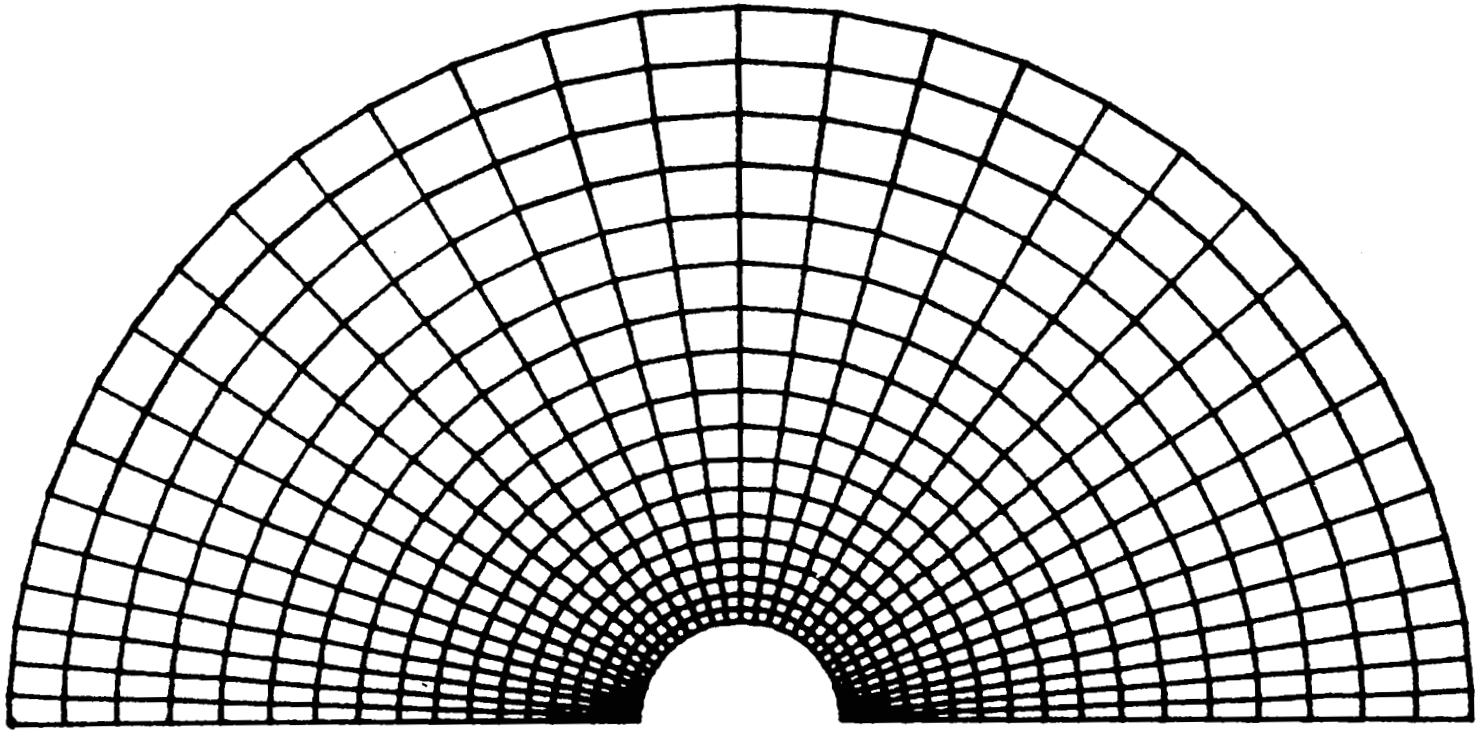

Figure 3b. - Circular cylinder coordinate system, $Re_D = 40$; far field (radial locations 17 through 35).

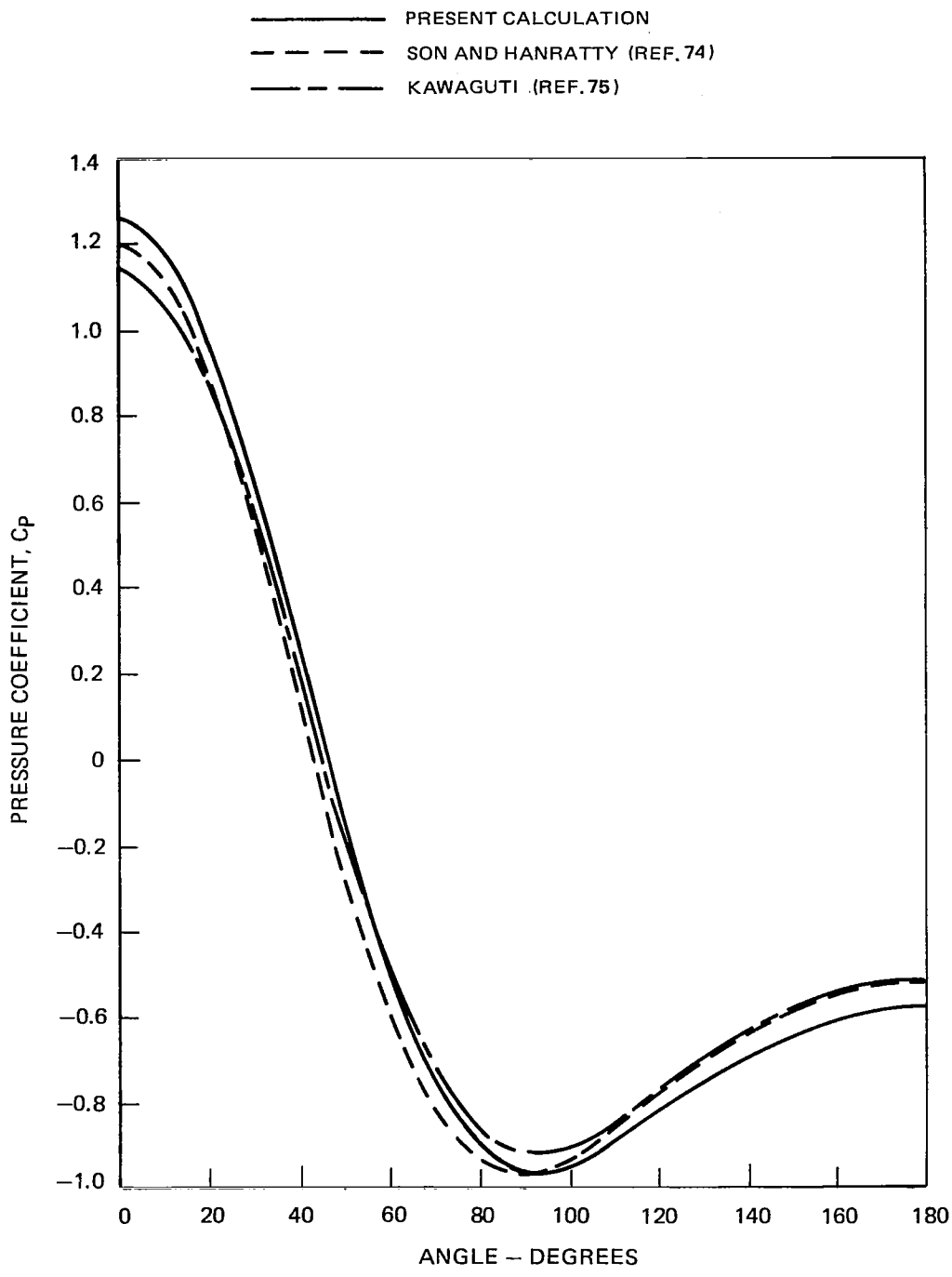

Figure 4.—Pressure distribution about circular cylinder, $Re_D = 40$.

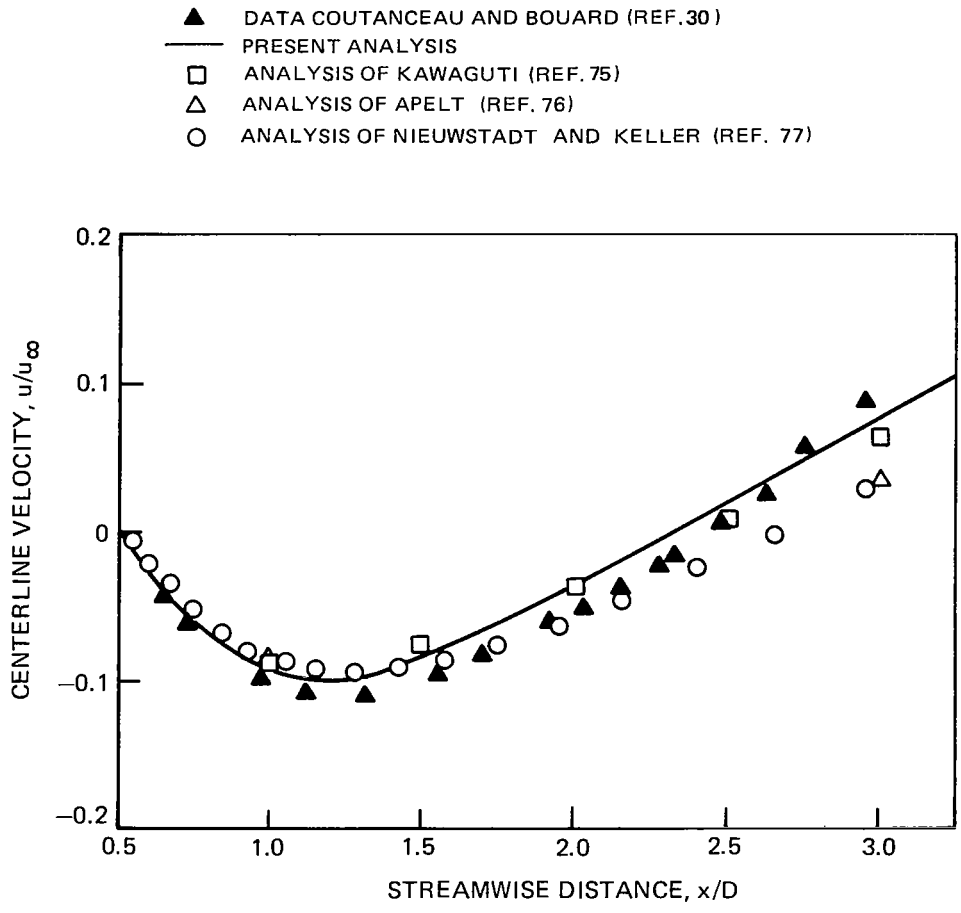

Figure 5. — Centerline velocity distribution behind circular cylinder, $Re_D = 40$.

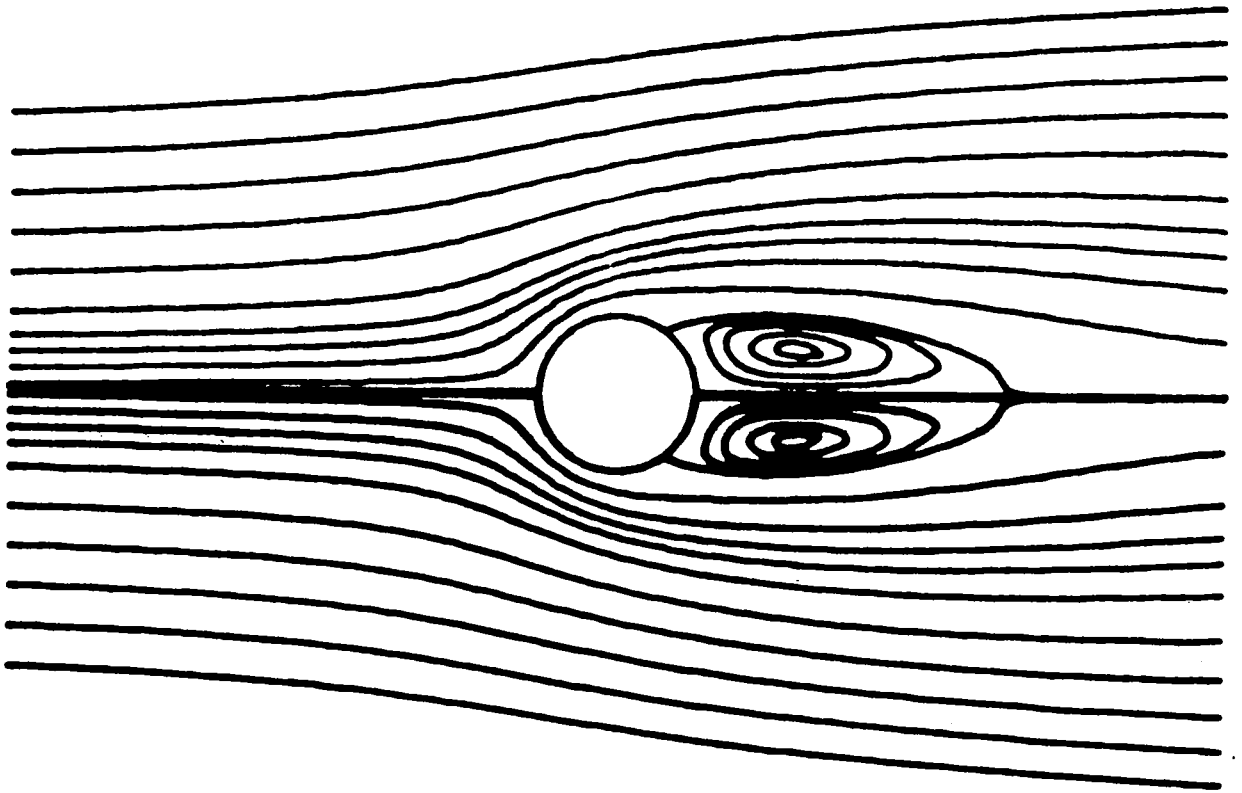

Figure 6. - Streamlines about circular cylinder, $Re_D = 40$.

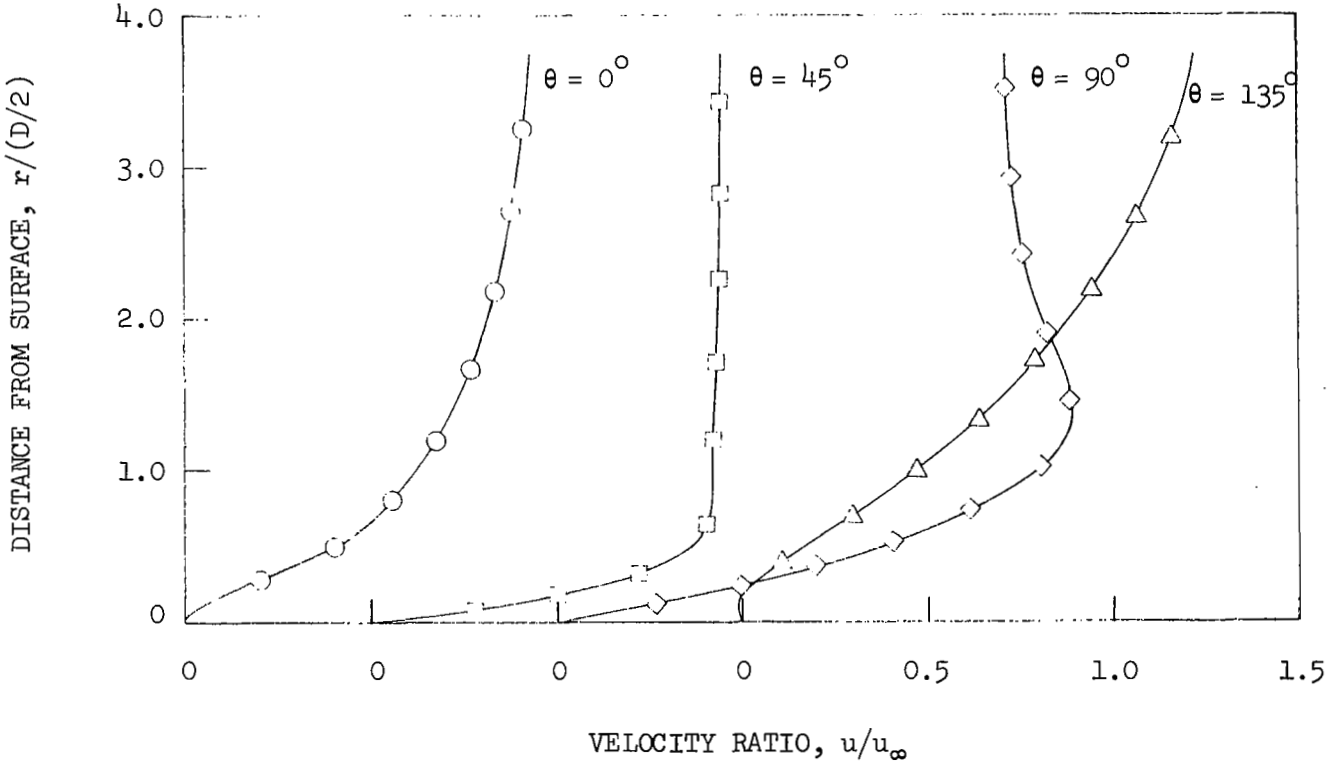

Figure 7. - Streamwise velocity profiles about circular cylinder, $Re_D = 40$.

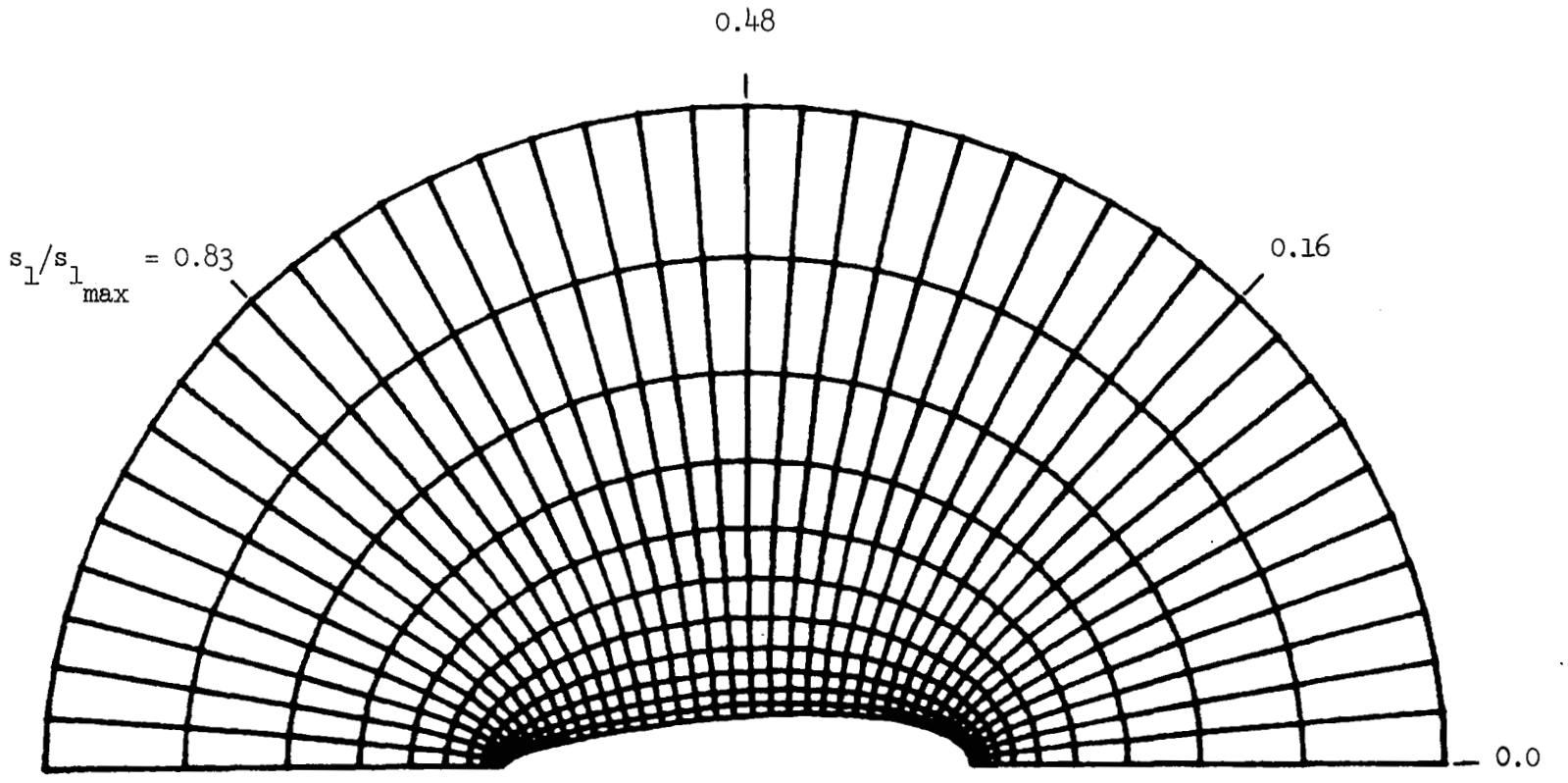

Figure 8a. - Joukowski airfoil coordinate system, Re_ℓ = 80; near field (pseudo radial locations 1 through 12).

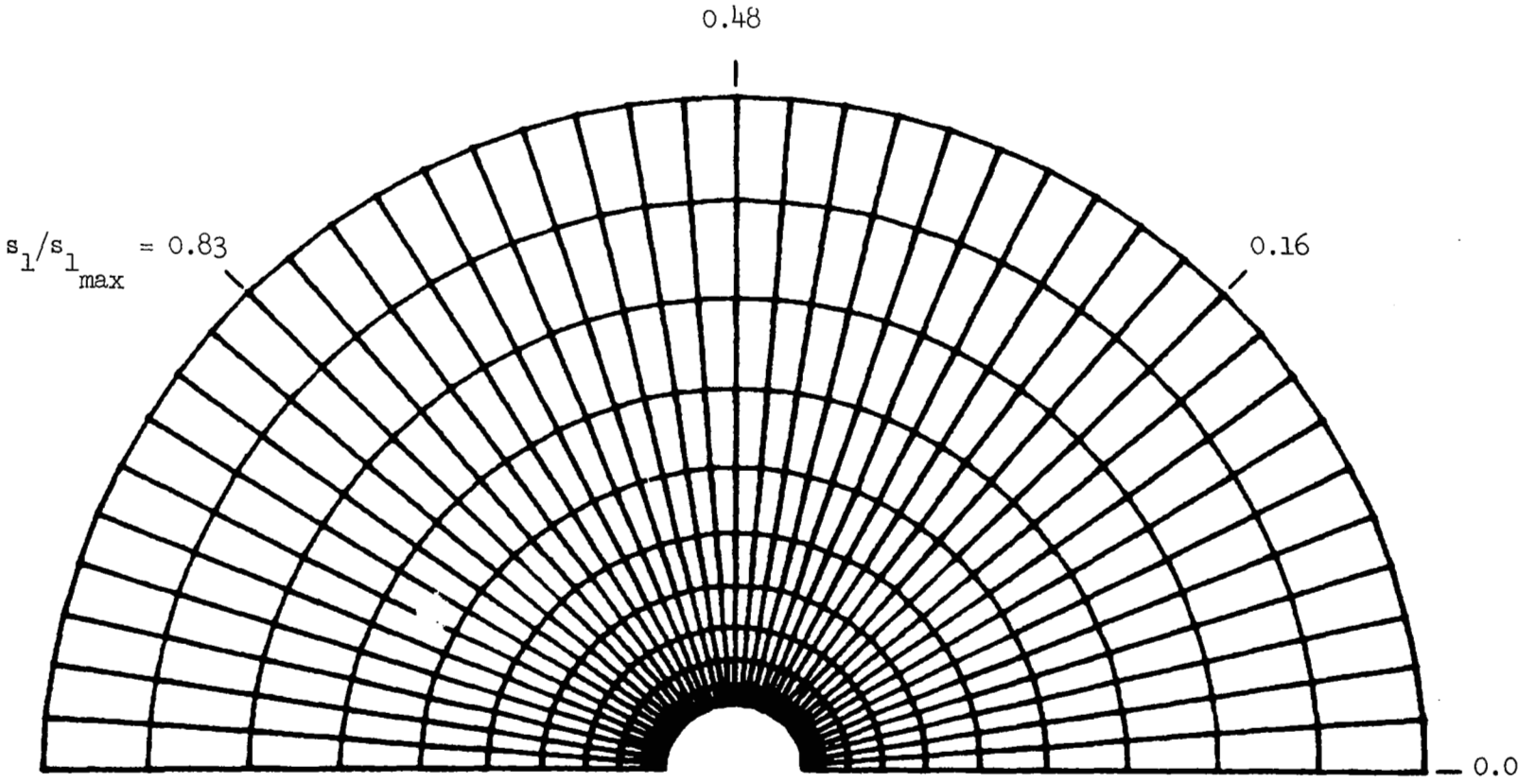

Figure 8b. - Joukowski airfoil coordinate system, Re_{ℓ} = 80; far field (pseudo-radial locations 12 through 22).

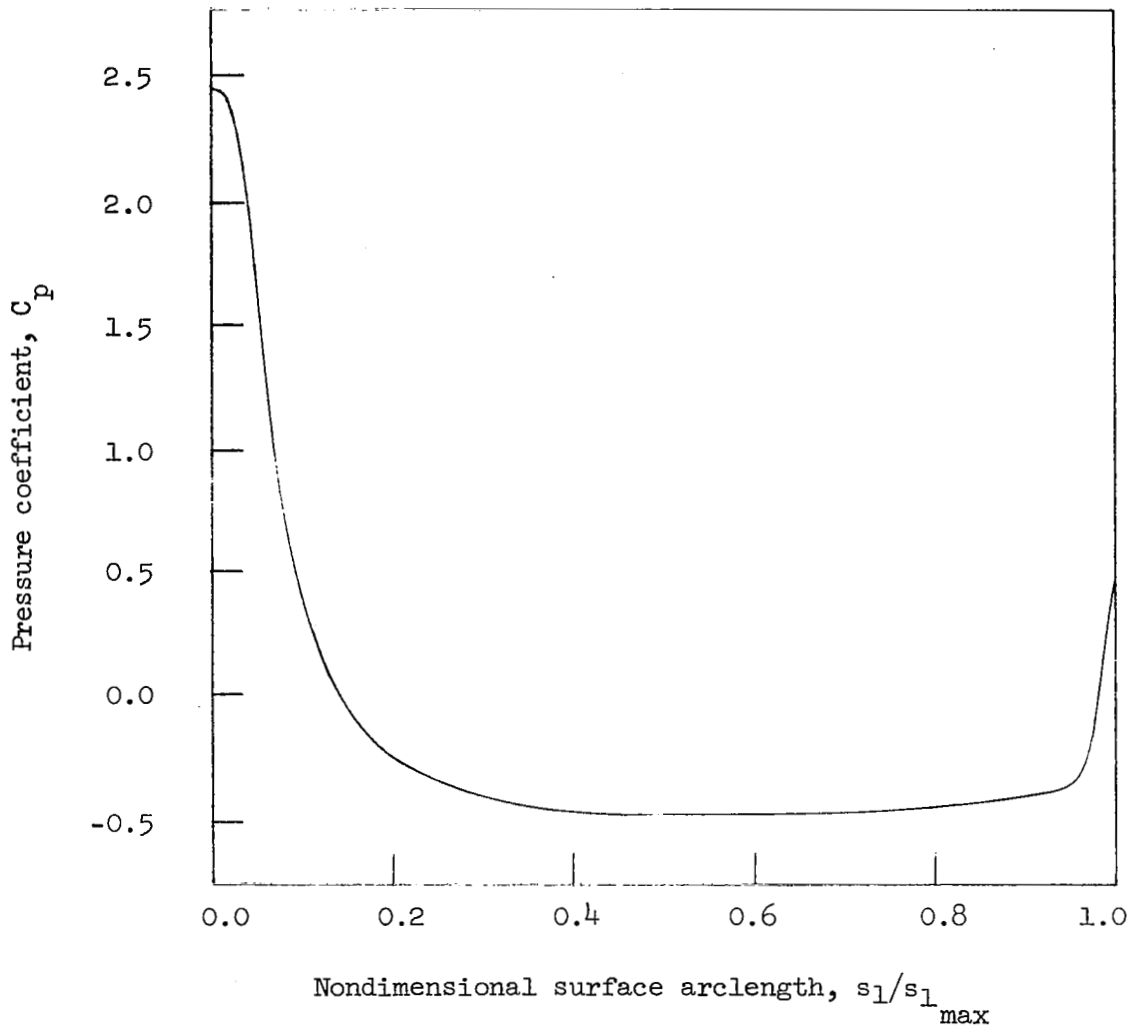

Figure 9. - Pressure distribution about Joukowski airfoil, $Re_\ell = 80$.

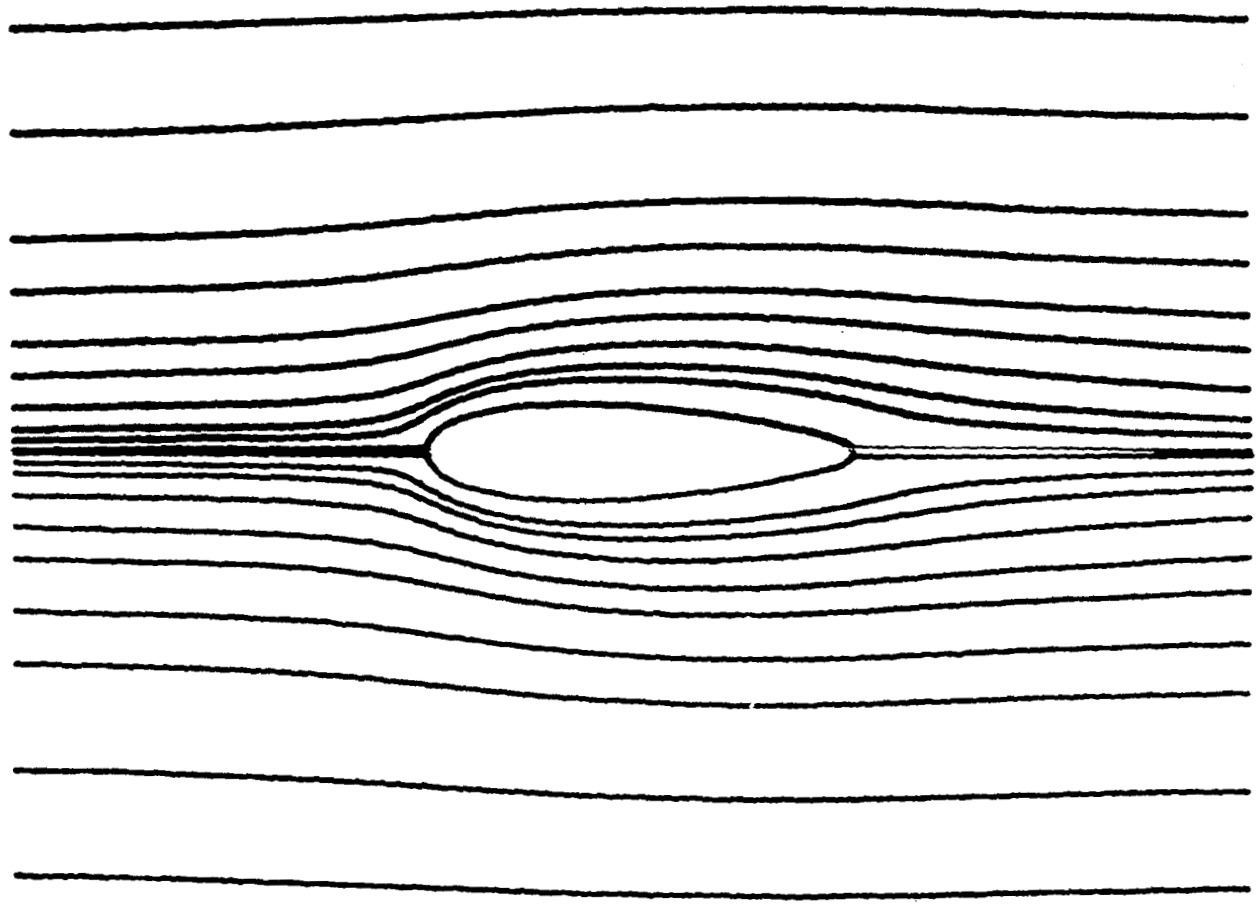

Figure 10. - Streamlines about Joukowski airfoil, $Re_{\ell} = 80$.

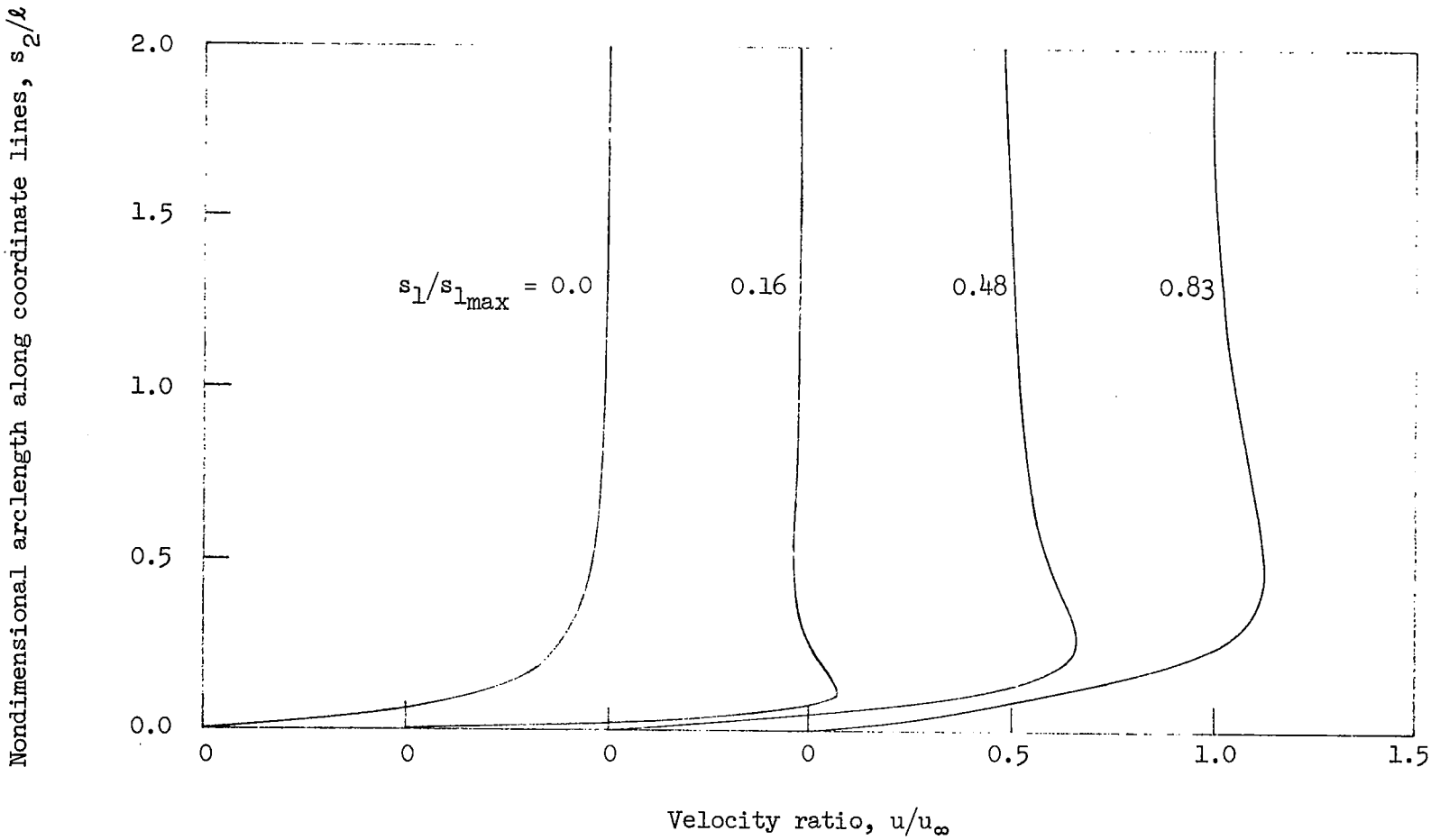

Figure 11. - Streamwise velocity profiles about Joukowski airfoil, Re_ℓ = 80.

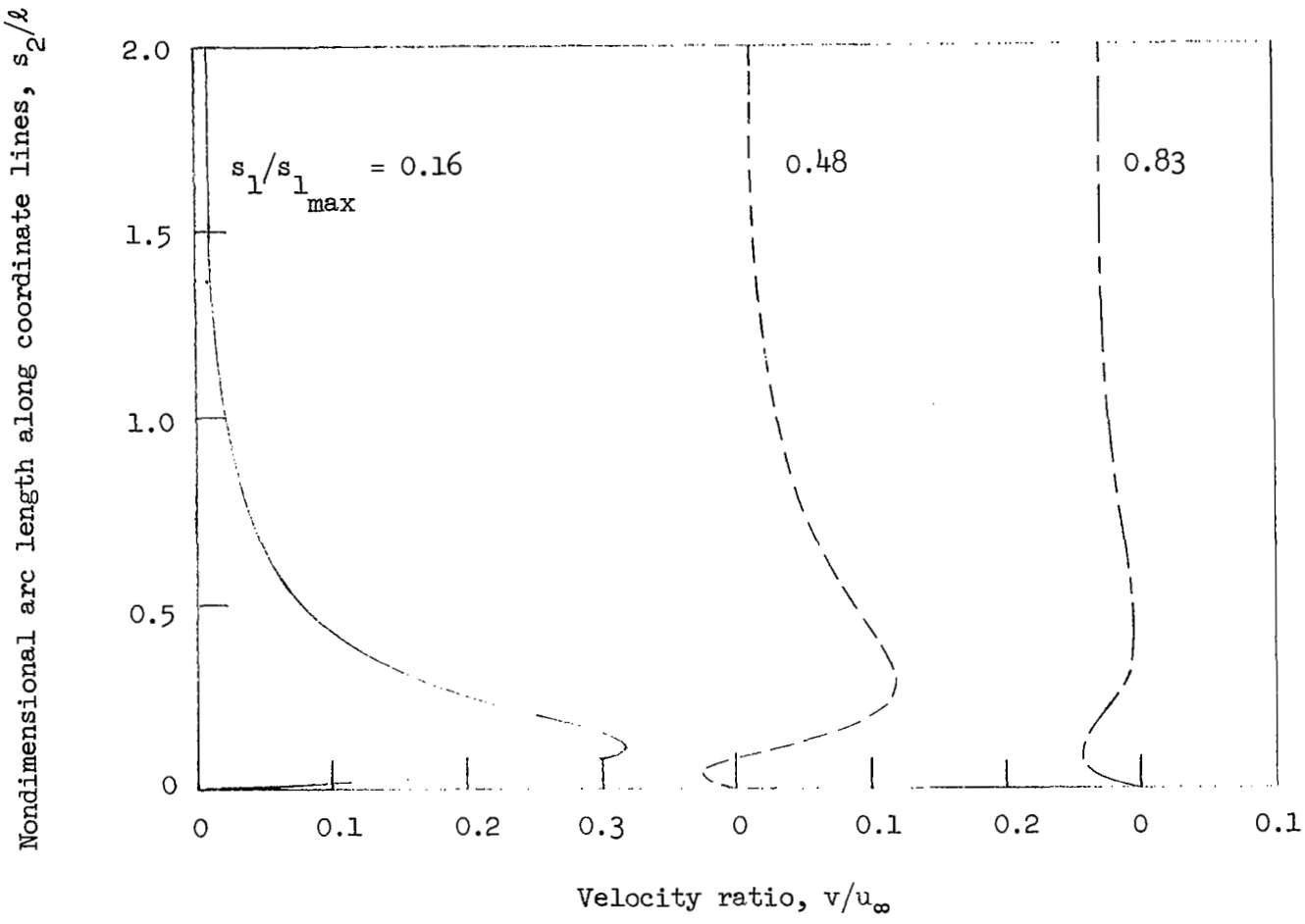

Figure 12. - Transverse velocity profiles about Joukowski airfoil, Re_ℓ = 80.

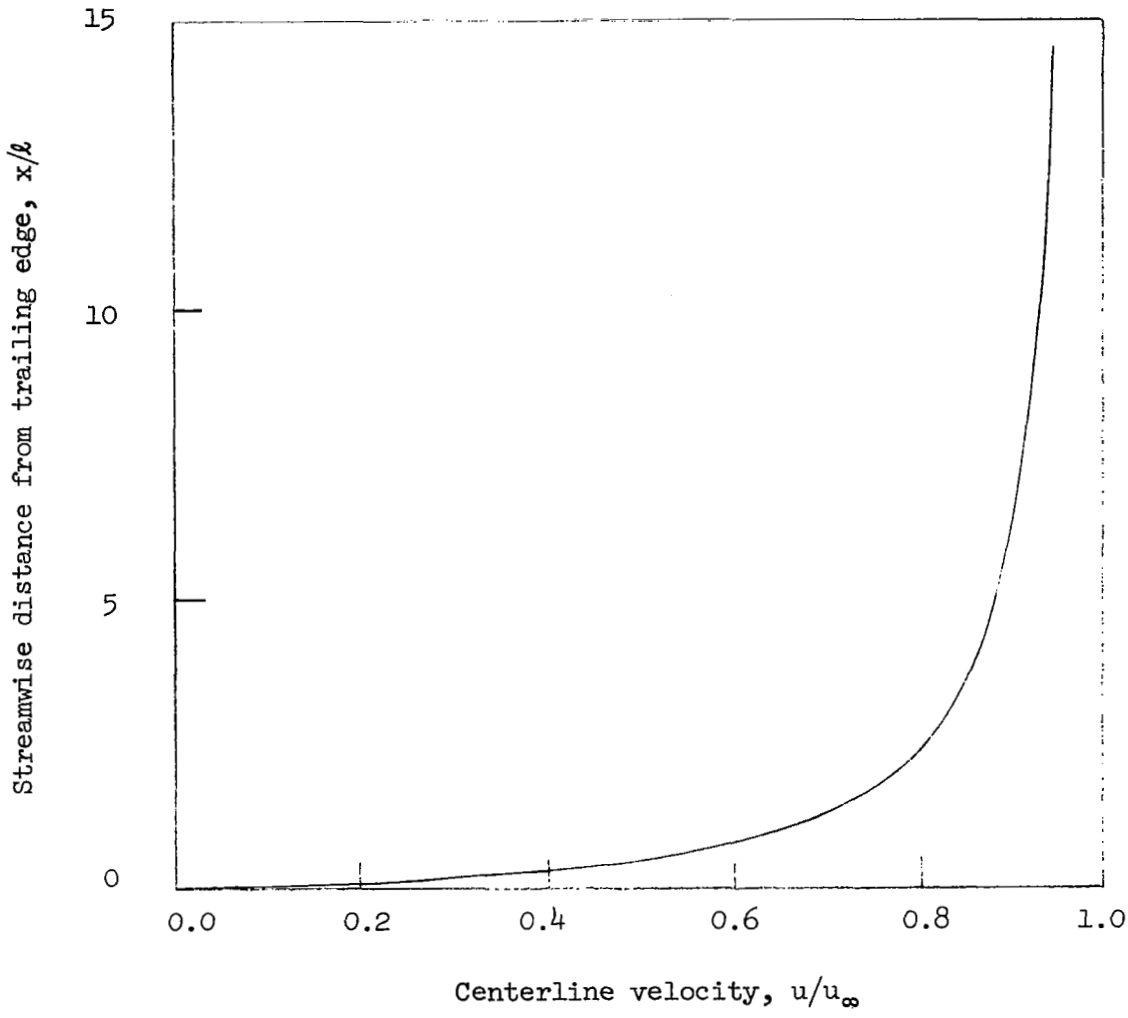

Figure 13. - Wake centerline velocity distribution behind Joukowski airfoil, $Re_{\ell} = 80$.

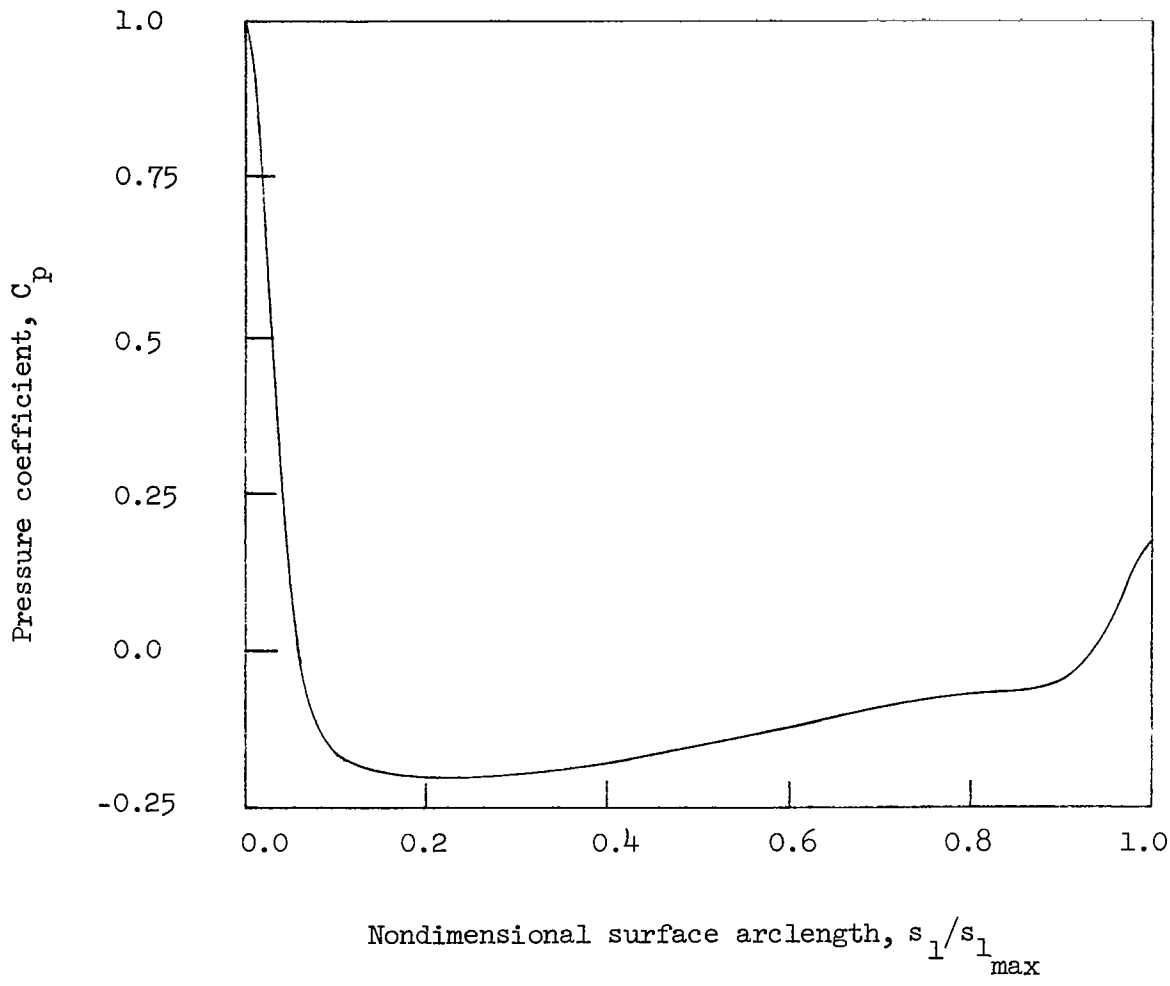

Figure 14. - Pressure distribution about Joukowski airfoil, $Re_\ell = 1000$ (not a converged solution).

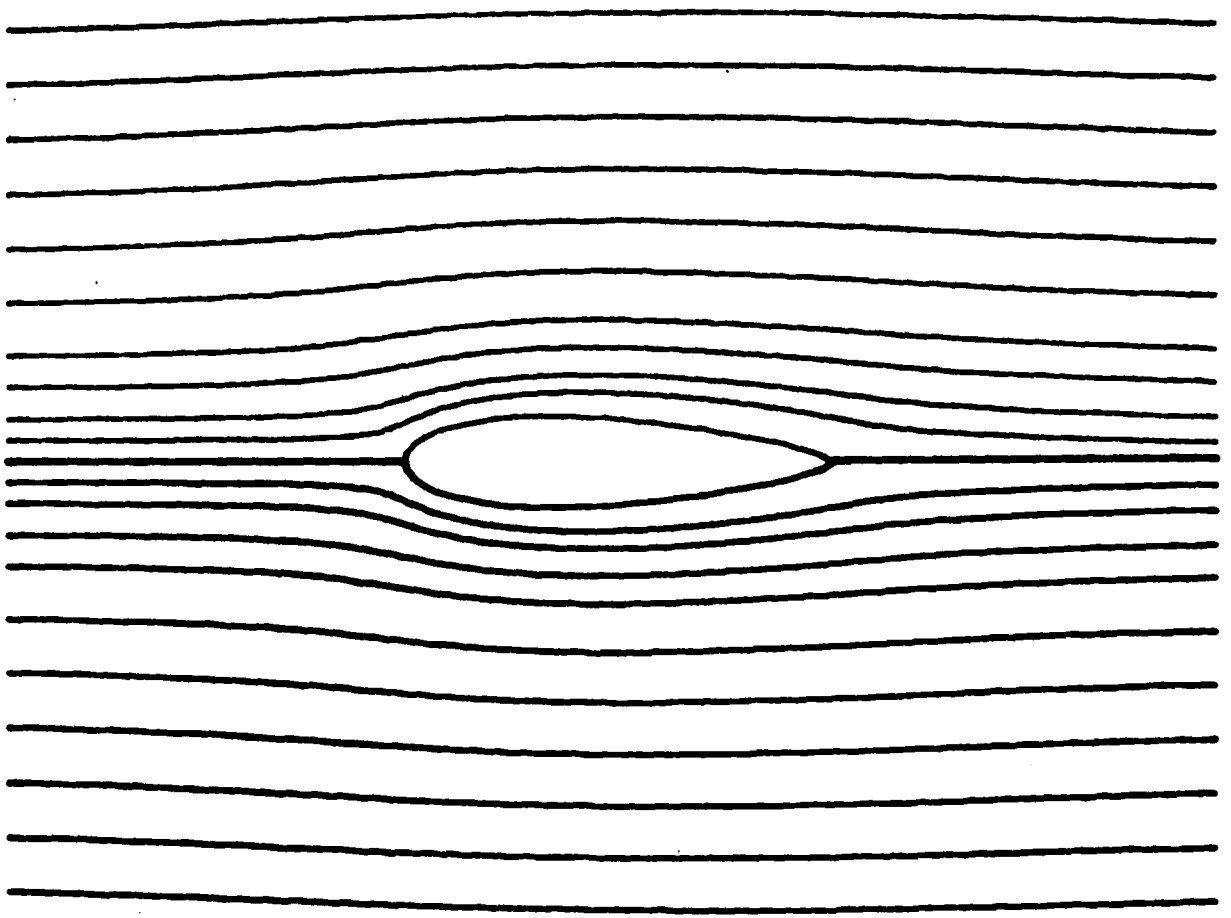

Figure 15. - Streamlines about Joukowski airfoil, Re_{ℓ} = 1000 (not a converged solution).

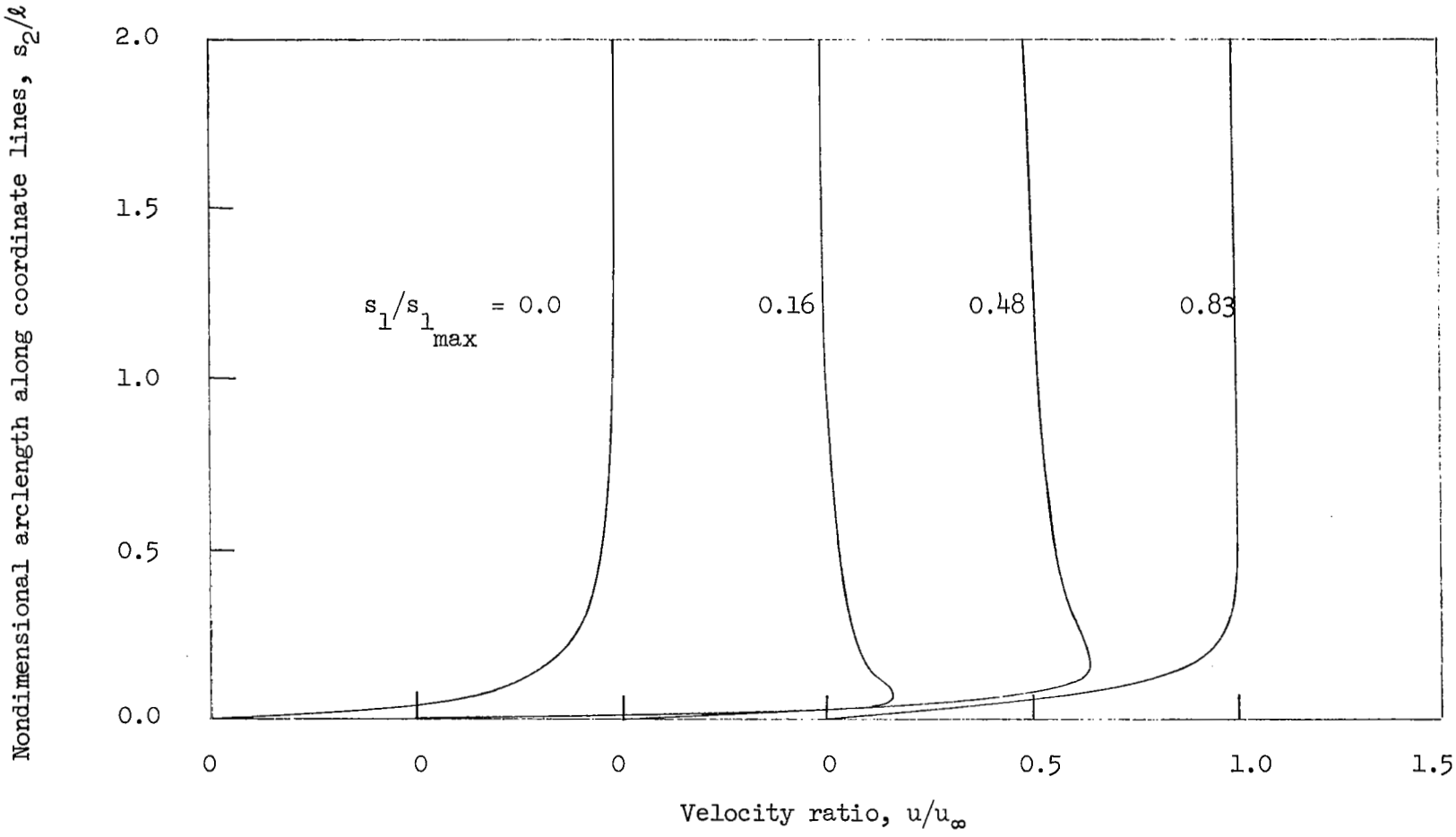

Figure 16. - Streamwise velocity profiles for Joukowski airfoil, Re = 1000 (not a converged solution).

1. Report No.	2. Government Accession No.	3. Recipient's Catalog No.
NASA CR-2969		

4. Title and Subtitle	5. Report Date
ANALYSIS OF STRONG-INTERACTION DYNAMIC STALL FOR LAMINAR FLOW ON AIRFOILS	April 1978
	6. Performing Organization Code
7. Author(s) H. J. Gibeling, S. J. Shamroth, and P. R. Eiseman	8. Performing Organization Report No. R77-912030-17
	10. Work Unit No.
9. Performing Organization Name and Address United Technologies Research Center East Hartford, CT 06108	11. Contract or Grant No. NAS1-13619
	13. Type of Report and Period Covered Contractor Report
12. Sponsoring Agency Name and Address National Aeronautics and Space Administration Washington, DC 20546	14. Sponsoring Agency Code

15. Supplementary Notes The contract research effort which has led to the results in this report was financially supported by U.S. Army Research and Technology Laboratories (AVRADCOM), Structures Laboratory.
Langley technical monitor: Warren H. Young, Jr. Final report.

16. Abstract

A compressible Navier-Stokes solution procedure is applied to the flow about an isolated airfoil. Two major problem areas have been investigated. The first area is that of developing a coordinate system and an initial step in this direction has been taken. An airfoil coordinate system obtained from specification of discrete data points has been developed and the heat conduction equation has been solved in this system. Efforts required to allow the Navier-Stokes equations to be solved in this system are discussed. The second problem area is that of obtaining flow field solutions. Solutions for the flow about a circular cylinder and an isolated airfoil are presented. In the former case the prediction is shown to be in good agreement with data.

17. Key Words (Suggested by Author(s))	18. Distribution Statement
Dynamic stall, Navier-Stokes, airfoil stall	Unclassified - Unlimited Subject Category 34

19. Security Classif. (of this report)	20. Security Classif. (of this page)	21. No. of Pages	22. Price*
Unclassified	Unclassified	70	$5.25

* For sale by the National Technical Information Service, Springfield, Virginia 22161 NASA-Langley, 1978